Elucidating the Role of COBRA in Plant Development in *Arabidopsis thaliana*

by

Karlson Pang

B.Sc., The University of British Columbia, 2015

A THESIS SUBMITTED IN PARTIAL FULFILLMENT OF

THE REQUIREMENTS FOR THE DEGREE OF

MASTER OF SCIENCE

in

THE FACULTY OF GRADUATE AND POSTDOCTORAL STUDIES

(Botany)

THE UNIVERSITY OF BRITISH COLUMBIA

(Vancouver)

August 2018

The following individuals certify that they have read, and recommend to the Faculty of Graduate and Postdoctoral Studies for acceptance, a thesis/dissertation entitled:

Elucidating the Role of COBRA in Plant Development in *Arabidopsis thaliana*

submitted by Karlson Pang in partial fulfillment of the requirements for

the degree of Master of Science

in Botany

Examining Committee:

Geoffrey Wasteneys
Supervisor

Xin Li
Supervisory Committee Member

Supervisory Committee Member

Cara Haney
Additional Examiner

Additional Supervisory Committee Members:

Supervisory Committee Member

Abstract

Cellulose is the most abundant biopolymer on Earth and was integral for evolution of land plants. Cellulose microfibrils are one of the primary components of plant cell walls, and are critical in maintaining anisotropic growth. These microfibrils are synthesized at the plasma membrane by cellulose synthases (CESAs). Alterations in cellulose biosynthesis, such as mutations in CESAs, can cause defects ranging from decreased unidirectional growth to embryonic lethality.

COBRA (COB) is an essential gene in *Arabidopsis thaliana* important for cellulose deposition and maintaining unidirectional growth, and is highly co-expressed with primary cell wall CESAs. Despite the importance of COB in cellulose biosynthesis, there is still little known about its role or function. This is primarily due to the lack of tools, such as reporter fusion constructs, to assess COBRA's localization, trafficking, and function. While a cYFP-conjugated COB reporter fusion construct (COB-cYFP) was recently made available, this construct could not fully complement the *cob-4* null mutant, casting doubt on any results obtained. However, using construct as a base I was able to improve its ability to complement *cob-4* in addition to generating plant lines that are more optimal for live-cell imaging (Chapter 3).

In addition to improving the COB-cYFP construct, I also generated a 6x histidine-tagged COB construct (HisCOB) that was able to fully complement the *cob-4* null mutant (Chapter 4). Using HisCOB, I was able to demonstrate that COB undergoes at least 2 cleavage events after its secretion to the apoplast, and that this cleaved peptide is ultimately endocytosed. Furthermore, I show evidence that the abundance of COB is too low for it to be a structural component of the cell wall as previously hypothesized, and instead COB likely plays a role in signaling and regulation of cellulose biosynthesis.

Finally, *cob* mutants were generated and investigated to identify potential COB functional domains that were previously uncharacterized (Chapter 5). I identified a region of the COB protein that may contain the primary cleavage site that allows COB to be endocytosed, and demonstrate the importance of the cellulose-binding domain for function. In addition, I provide evidence that COB likely functions as a homodimer.

Lay Summary

Cellulose is a biopolymer made of linked glucose sugars. It is an essential component of the plant cell walls that surround every plant cell. Cellulose is produced at the surface of cells by enzymes called cellulose synthases which extrude cellulose into the cell wall. In addition to cellulose synthases, other proteins also play an important role in producing cellulose. One such protein is COBRA, which has been shown to be essential for cellulose production. Despite the importance of COBRA its function is still unknown, mostly in part due to the lack of tools to properly localize it and assess its function. Using a COBRA-reporter fusion construct I generated, I was able to show that COBRA likely plays a role in monitoring the cellulose produced by the cellulose synthases and maintaining overall cell wall integrity. In addition, I also provide a new model on COBRA's trafficking and how that relates to function.

Preface

The Arabidopsis *cobra-4* (*cob-4*) knock-out T-DNA insertion lines were obtained from the Syngenta Arabidopsis Insertion Library (SAIL) collection (SAIL 735D10) (Roudier et al., 2005). The *cob-1* point mutant lines were obtained from the Arabidopsis Biological Resource Center (ABRC) (Hauser, Morikami, & Benfey, 1995). The COB-HA in *hulk-1* plant line was obtained from Dr. Georg Seifert (unpublished) (The University of Natural Resources and Life Sciences, Vienna) and the out-crossing of the *hulk-1* background performed by Dr. Miki Fujita (Wasteneys lab, UBC). The endosomal marker lines wave_129R and wave_2R were obtained from Niko Geldner (University of Lausanne) (Geldner et al., 2009). *COBpro*::*COB-dcYFP* plasmid construct was provided by Dr. Miki Fujita (unpublished). The primers used for site-directed mutagenesis of cYFP were also designed by Dr. Miki Fujita.

In chapters 3 and 4, the cellulosic glucose assays were performed by Dr. Miki Fujita and Dr. Charles Hocart (Australian National University). In chapter 4 the COB-mcYFP in *cob-4* protein extraction and immunoblot were performed by Sim Lahar and Dr. Miki Fujita. Also in chapter 4, running of the LC-MS/MS and analyses of the mass spectrometry data were performed by Jenny Moon (Foster lab, UBC). In chapter 5, segregation of homozygous COB-mcYFP and HisCOB in wild-type background lines were performed by Dr. Miki Fujita.

All other experiments and data analysis were performed by Karlson Pang.

Table of Contents

List of Tables

List of Figures

List of Symbols

35S	Cauliflower mosaic virus 35S
BASTA	Glufosinate
ºC	Degrees Celsius
μmol $m^{-2}s^{-1}$	Photosynthetic photon flux density

List of Abbreviations

6xHis	6x-Histidine
BC1	Brittle Culm1
BLAST	Basic Local Alignment Search Tool
CBD	Cellulose-binding domain
CESA	Cellulose synthase
CMU	CELLULOSE-MICROTUBULE UNCOUPLING
COB	COBRA
COBL	COBRA-like
cPCR	Colony PCR
CSC	Cellulose synthase complex
CSI1	CELLULOSE SYNTHASE INTERACTING1
cYFP	Citrine yellow fluorescent protein
E. coli	Escherichia coli
g	Gram
Gal*p*A	Galacturonic acid
GC-MS	Gas-chromatography mass spectrometry
gCOB	Genomic COBRA
GPI	Glycosylphosphatidylinositol
HA	Human influenza hemagglutinin
HG	Homogalacturonan
IMAC	Immobilized metal affinity chromatography

kDa	Kilodalton
LB	Lysogeny broth
LC-MS/MS	Liquid-chromatography mass spectrometry/mass spectrometry
M	Molar
MED16	MEDIATOR16
MF	Microfibril
mL	Milliliter
mM	Millimolar
paGFP	Photoactivable green fluorescent protein
pBKS	pBluescript KS (-)
pCA2300	pCAMBIA 2300
PMEI	Pectin methylesterification inhibitors
RFP	Red fluorescent protein
RG-I	Rhamnogalacturonan I
RG-II	Rhamnogalacturonan II
RNA	Ribonucleic acids
RNAseq	RNA sequencing
rpm	Rotations per minute
SAIL	Syngenta Arabidopsis Insertion Library
SDS-PAGE	Sodium dodecyl sulfate polyacrylamide gel electrophoresis
SFR6	SENSITIVE-TO-FREEZING6
SOB	Super optimal broth

TA	Thaxtomin A
TBS	Tris-buffered saline
TBST	Tris-buffered saline and Tween
TCA	Trichloroacetic acid
TEM	Transmission electron microscopy
UDP-glucose	Uridine diphosphate glucose
XG	Xyloglucan
µg	Microgram
µL	Microliter

Acknowledgements

I would like to sincerely thank my supervisor, Dr. Geoffrey Wasteneys for his mentorship, support, and patience over the course of these last few years. I am extremely grateful to him for this learning opportunity. I would also like to thank my supervisory committee members, Dr. Xin Li and Dr. Reinhard Jetter for their guidance and advice.

This project could not have been accomplished without the mentorship and guidance of Dr. Miki Fujita who has been a great research mentor and it is due to her that I am in Geoff's lab today. I would also like to thank all members of the Wasteneys and Samuels lab for all their support throughout the past few years. To my previous undergraduate assistants, Jeremy Soroka and Sonia Sharma, thank you for helping me at various stages of my projects, especially in the generation of constructs and plant lines.

I am also thankful to Dr. Leonard Foster and Jenny Moon of the Foster lab at the University of British Columbia for their assistance in teaching me protein mass spectrometry. I am also thankful to Dr. Charles Hocart at the Australian National University for his assistance with the cellulosic glucose analyses.

I am grateful to the Botany department staff and fellow graduate students for their assistance and encouragement. I would also like to thank the UBC Bioimaging facility for their assistance and training on the spinning disc confocal and the two-photon microscope.

I am also forever grateful to my family and friends for their love, support, and words of encouragement.

Chapter 1: Introduction

1.1 Overview

Colonization of land by plants is strongly associated with the evolution of rigid cell walls. With both tension- and load-bearing properties, cell walls enable plants to withstand the enormous pressures required for plant growth, and reinforce specialize vascular and fibre cells to enable plants to grow against the forces of gravity. In addition, cell walls also serve to inhibit excessive water loss and to enable cell-to-cell communication, allowing plants to function as multicellular organisms (Popper et al., 2011). Cell walls can be classified as either primary cell walls, which surround all plant cells and are deposited during cell expansion, or secondary cell walls, which are deposited under the primary cell, generally after cell expansion. Plant primary cell walls are mainly composed of the polysaccharides cellulose, hemicellulose, and pectin. Proper deposition and organization of cellulose, the major tension-bearing component of the cell wall, is integral for maintaining the structure and function of plant cell walls, though the mechanisms underlying this ordered deposition are still unknown.

Proteins that are situated on the outer leaflet of the plasma membrane, such as glycosylphosphatidylinositol (GPI) anchored proteins, are in an ideal position to modulate newly synthesized cellulose as it is extruded from the cellulose synthase complexes (CSCs). The *COBRA* (*COB*) gene family is a group of glypiated proteins that have been suggested to play a role in cellulose biosynthesis, as *cob* mutants have cellulose deficient phenotypes, though their exact function is still unknown. Each member of the *COB* gene family contains at least one cellulose-binding domain (CBD) at the N-terminus of the protein, allowing for direct interaction(s) with cellulose at the plasma membrane (Roudier, Schindelman, DeSalle, & Benfey, 2002). This allows COBRA, and the COBRA-likes (COBLs), to potentially modulate

cellulose biosynthesis by directly binding newly synthesized cellulose at the point of extrusion. However, the specific characteristics of cellulose microfibrils (MFs) in the primary cell wall that are influenced by COBRA are unknown.

1.2 Plant cell walls

In order to properly place COBRA at its appropriate functional position in the production of cellulose, it is necessary to first understand cellulose biosynthesis in regards to cell wall structure and development. The primary cell wall polysaccharides include cellulose, pectins, and hemicelluloses (Figure 1.1).

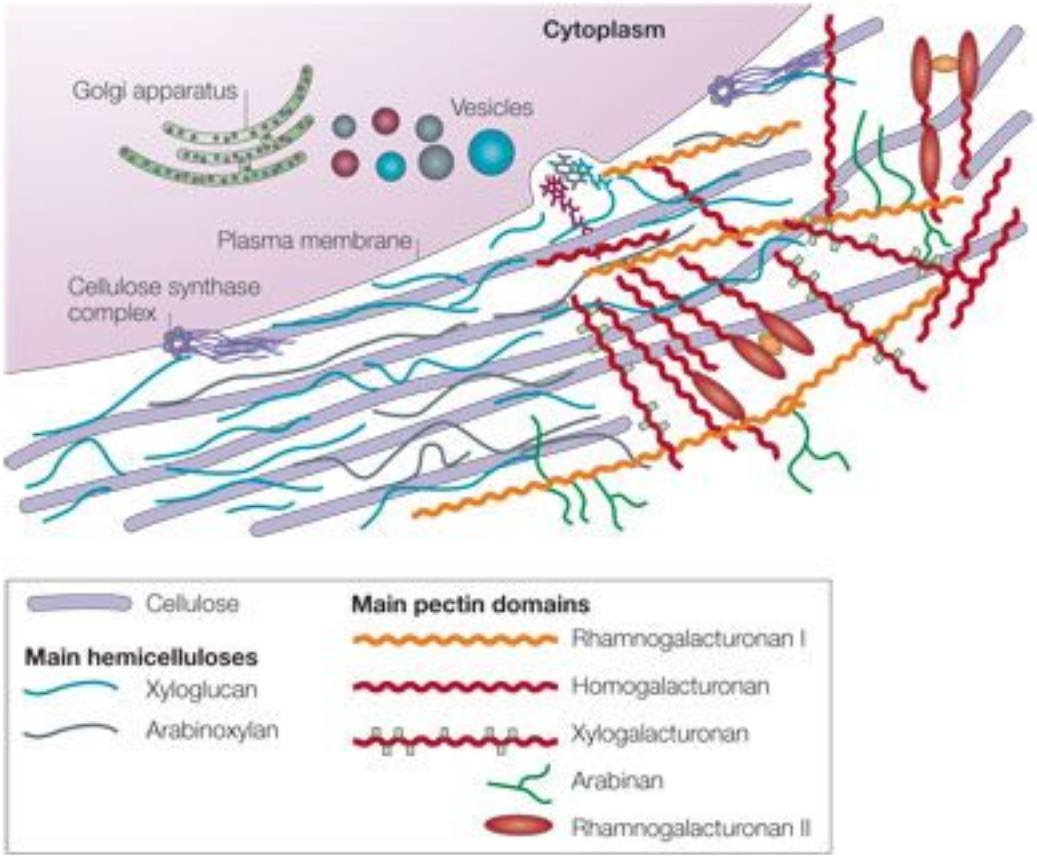

Figure 1.1. Polysaccharides of the Primary Plant Cell Wall

The plant primary cell wall is composed of the polysaccharides cellulose, hemicelluloses, and pectins. Adapted from "Growth of the primary cell wall," by D.J. Cosgrove, 2005, *Nature Reviews Molecular Cell Biology*, *6*, p. 852. Copyright 2018 by Springer Nature Limited

Cellulose consists of β-(1-4)-linked d-glucose chains deposited in a parallel orientation, which can then form both intra- and inter-chain hydrogen bonds resulting in regions of high crystallinity within the polymer. Current research suggests that 18-24 glucan chains form an elementary fibril, which in turn condense into MFs (Cosgrove, 2014; Fernandes et al., 2011; Newman, Hill, & Harris, 2013). The crystalline structure of cellulose leads to tightly packed chains of cellulose within MFs, and it is also hypothesized that the degree of polymerization within the glucan chains influences crystallinity (Hallac & Ragauskas, 2011).

Pectins are a type of plant cell wall polysaccharide characterized by an α-(1-4)-linked d-galacturonic acid (Gal*p*A) backbone, and makes up approximately 35% (w/v) of the primary cell wall in dicots (Mohnen, 2008). Pectins can be split into three major types: homogalacturonan (HG), rhamnogalacturonan I (RG-I), and substituted galacturonan rhamnogalacturonan (RG-II) (Atmodjo, Hao, & Mohnen, 2013). HG is a polymer of α-(1-4)-linked d-galacturonic acid and accounts for over 60% of pectins found in the primary cell walls (Ridley, O'Neill, & Mohnen, 2001). HG Gal*p*A residues may be methyl-esterified at the C-6 carboxyl, and this methylesterification is hypothesized to be tightly regulated during plant development and in the plant immune response (Lionetti, Cervone, & Bellincampi, 2012; Wolf, Mouille, & Pelloux, 2009). HG has also been shown to be covalently linked to both RG-I and RG-II, and is hypothesized to covalently cross-link to xyloglucan (XG) polysaccharides (Caffall & Mohnen, 2009). In the model dicot *Arabidopsis thaliana* (hereafter Arabidopsis), mutants with inhibited pectin biosynthesis have been shown to have primary cell walls with significantly weaker mechanical properties and to be more vulnerable to plant pathogens (Bethke et al., 2016).

Hemicelluloses are heteropolymers with varying structures and biochemical properties. The exact definition of hemicelluloses is not well defined, but the term is generally used to

denominate cell wall polysaccharides that are characterized as being neither cellulose nor pectin, and by having β-(1-4)-linked backbones of glucose, xylose, or mannose (Scheller & Ulvskov, 2010). Xyloglucans (XGs) are the most abundant hemicellulose in dicotyledonous cell walls, comprising up to 20-25% of the primary cell wall (Hayashi, 1989). XGs typically consist of a β-(1-4)-linked d-glucose backbone with branching d-xylose side chains in an α-d-Xyl-(1,6)-Glc conformation, with the occasional d-galactose or l-fucose residue (Scheller & Ulvskov, 2010). Hemicelluloses can bind directly to both the hydrophobic and hydrophilic surfaces of elementary cellulose fibrils, cross-linking them to provide rigidity to the cell wall (Park & Cosgrove, 2012). In Arabidopsis, mutants lacking XG have been shown to possess primary cell walls that have an altered cell wall composition in addition to significantly weaker mechanical properties (Cavalier et al., 2008).

1.3 Primary cell walls

Plant cell walls provide structural support to plant cells and define cell shape. The primary cell wall is deposited during in dividing and elongating cells, and defines the final cell shape in the majority of cell types. As such, the primary cell wall is selectively malleable in order to enable cell expansion to occur through a process of regulated deformation termed anisotropic growth. Anisotropic growth underlies plant cell morphology and function, and is achieved by remodeling of the primary cell wall to prevent isotropic cell wall expansion. Plant cells can elongate either by tip growth, where growth occurs from a small region at one end of the cell, or diffuse growth, where cell wall polysaccharides are deposited perpendicular to the axis of cell expansion (Laurie & David, 2005). Cell wall loosening is achieved by a suite of proteins and enzymes (expansins, cellulases, xyloglucan endotransglycolase/hydrolase, endo-(1-

4)-β-d-glucanase, pectinases, and polygalactanases) as well as hydroxyl radicals that modify the cell wall polymers (Cosgrove, 2000, 2005; Park & Cosgrove, 2012).

1.4 Cellulose biosynthesis

Cellulose is synthesized at the plasma membrane by a family of glucosyltransferases known as cellulose synthases (CESAs), which associate together as multi-protein complexes (Cosgrove, 2005). In Arabidopsis, 10 CESAs family members have been identified and classified into two groups depending on their role in the synthesis in the primary or secondary cell wall. CESA1 to 3, CESA 5 and 6, and CESA 9 and 10 have been found to function specifically in primary cell wall formation, with CESA1 and CESA3 being essential while CESA6 is redundant with CESA2, CESA5, and CESA9 (Burn, Hocart, Birch, Cork, & Williamson, 2002; Desprez et al., 2007; S Li, Bashline, Lei, & Gu, 2014). CESA4, CESA7, and CESA8 are non-redundantly required for secondary cell wall synthesis (Timmers et al., 2009). Loss-of-function mutants in CESA1 and CESA3 are gamete lethal, while milder defects in either of these genes resulted in a reduction of cellulose biosynthesis and in cellulose-deficient phenotypes, such as dwarfism, root swelling, and ectopic lignification (Burn et al., 2002; Desprez et al., 2007).

CesAs self-assemble into cellulose synthase complexes (CSCs) in a hexamer rosette structure, each consisting of multiple CesA subunits. In the primary cell wall, CESA1 and CESA3 are required to form a functional CSC, in addition to at least one CESA6-like protein (Burn et al., 2002; Desprez et al., 2007). The CSC catalyzes the polymerization of UDP-glucose, produced by the cleavage of sucrose by sucrose synthase, into β-(1-4)-linked glucan chains (Coleman, Yan, & Mansfield, 2009; McNamara, Morgan, & Zimmer, 2015). Following polymerization of UDP-glucose within the CSC, the glucan chains are then extruded into the apoplast where they rapidly self-assemble into elementary fibrils. The extraction of the glucan

chains is thought to facilitate the propulsion of the CSCs through the plasma membrane, and CSC velocity is thought to be directly correlated with the speed of cellulose synthesis (Diotallevi & Mulder, 2007).

Changes in the polymerization rate have also been shown to be associated with changes in the crystallinity of cellulose. In wild type plants, crystallinity decreases as CSC velocity increases and CSC velocity is thus thought to be important for maintaining growth anisotropy. In contrast, this inverse correlation is lost in mutants with defects in growth anisotropy. In the *mor1-1* temperature-sensitive mutant, crystallinity and CSC velocity both increase at the restrictive temperature, while in the *cesa1*^{any1} mutant crystallinity and CSC velocity are both reduced (M Fujita et al., 2011, 2013). In contrast, in the *cesa1*^{aegeus} and *cesa3*$^{ixr1-2}$ mutants cellulose crystallinity decreases as CSC velocities increase (Harris et al., 2012). In addition, reductions in cellulose crystallinity and increases in CSC velocity has also been observed during rapid growth, such as during periods of elevated temperature (M Fujita et al., 2011). It is thus still unclear how changes in CSC velocity can affect cellulose crystallinity or how cellulose crystallinity can affect the rate of cellulose biosynthesis.

Numerous proteins in Arabidopsis have been identified that, when absent or non-functional, lead to changes in cellulose biosynthesis in the primary cell wall such as: KORRIGAN (Vain et al., 2014), COBRA (Roudier et al., 2005), STELLO 1 and 2 (Zhang et al., 2016), CELLULOSE SYNTHASE INTERACTING 1 (Gu et al., 2010), and CELLULOSE SYNTHASE MICROTUBULE UNCOUPLING 1 and 2 (Z. Liu et al., 2016). These studies depict cellulose synthesis as a concert of tightly regulated biosynthetic machinery (Figure 1.2). It is still unclear how the final structure of cellulose is determined, but alteration in the function of a single protein in the biosynthesis machinery likely alters cellulose structure. Examination of

each of the loss-of-function plant lines would help resolve the function of each of the components and elucidate that relationship between various components of cellulose biosynthesis and deposition. The *COBRA* gene family, which is known to function specifically in either primary or secondary cell wall deposition, is a key example of how cellulose biosynthesis-associated proteins can influence cellulose structure (Roudier et al., 2005; Atmodjo et al., 2008)

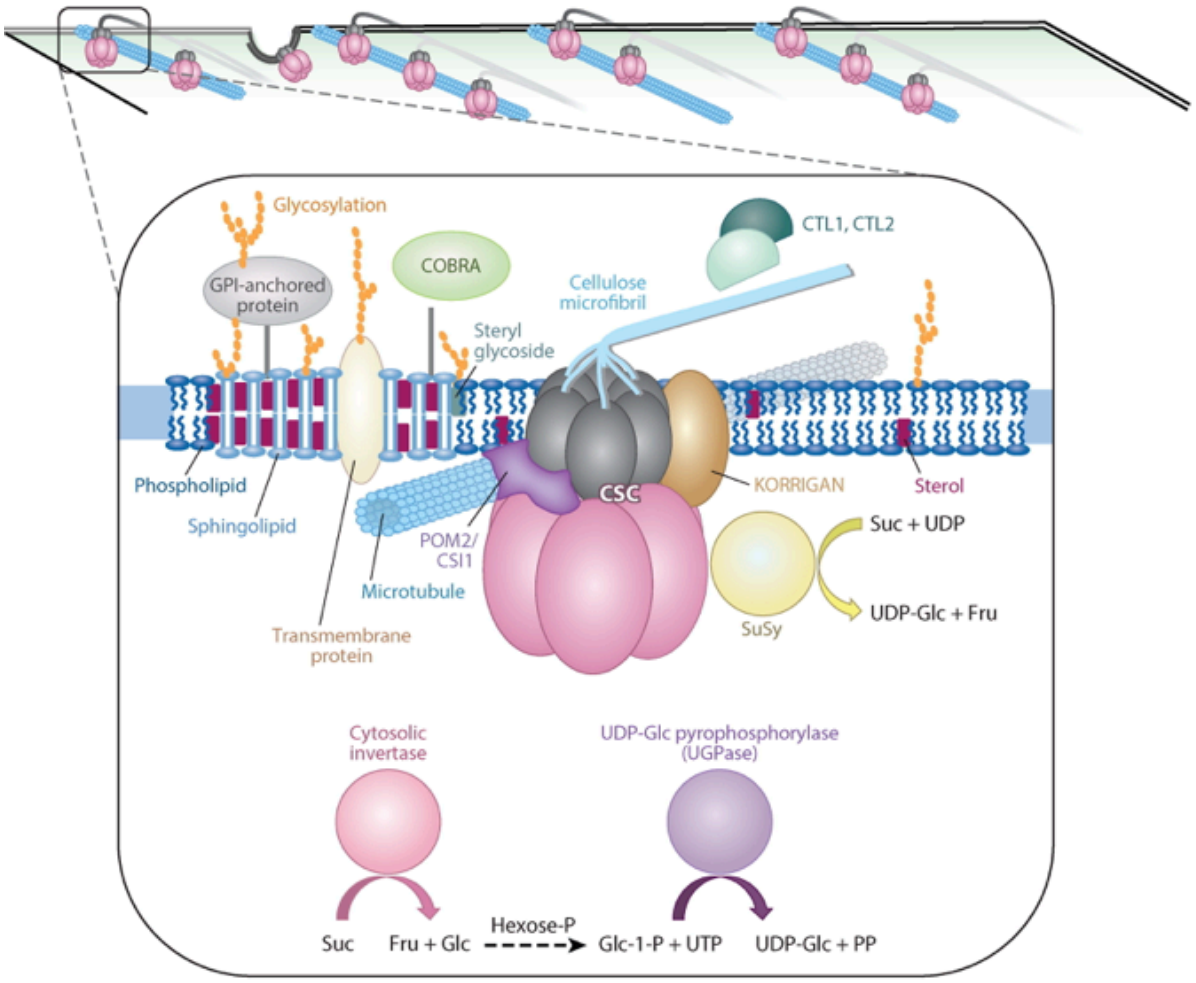

Figure 1.2. Influencers of Cellulose Biosynthesis

Cellulose is synthesized by the CSCs in a concert of tightly regulated biosynthetic machinery. CSC-interacting proteins such as KORRIGAN and CSI1 have been shown to directly affect the movement of the CSCs, while extracellular proteins such as COBRA and CTL1/2 can also affect CSC biosynthesis. Reprinted from "The Cell Biology of Cellulose Synthesis," by H.E. McFarlane, A. Doring, and S. Persson., 2014, *Annual Review of Plant Biology, 65,* p. 81. Copyright 2014 by Annual Reviews.

1.5 The *COBRA* gene family

COBRA genes have been identified as being important to cell wall and cellulose biosynthesis in all Viridaeplantae investigated to date. The Arabidopsis *COBRA* gene family consists of 12 members: the original *COBRA* (*COB*) and *COBRA-LIKE* (*CBL*) 1-11 (Roudier et al., 2002). Nine family members have been identified in maize (Brady, Song, Dhugga, Rafalski, & Benfey, 2007), 11 in rice (Y. Li et al., 2003), 18 in poplar (Ye, Kang, Osburn, & Cheng, 2009), and 17 in tomato (Cao, Tang, Giovannoni, Xiao, & Liu, 2012). COBRA family members contain at least one putative cellulose-binding domain (CBD) downstream of the N-terminal signal cleavage site, which has been used to separate the gene family into two subgroups based on the number of CBDs. The first group consists of *COB* and *COBL1-6*, each containing a single CBD, while the second group, consisting of *CBL7-11*, has an additional ~170 amino acids downstream of the N-terminal signal cleavage site containing an additional CBD upstream of the conserved CBD found in all *COB* family members (Roudier et al., 2002).

1.5.1 COBRA

The GPI-anchored protein COBRA (COB) was first identified in Arabidopsis as playing a role in conditional root expansion, as *cob-1* mutants had an abnormal root formation phenotype when seedlings were grown on high sucrose medium, whereby root cells underwent radial instead of longitudinal expansion (Benfey et al., 1993). The resulting morphology resembled the hood of a cobra snake, inspiring the name of the gene family. Further studies showed that the defects caused by *cob-1* were observed only in the roots, while aerial organs had normal development (Benfey et al., 1993; Schindelman et al., 2001). However, the *cob-1* allele is only a partial loss-of-function mutant that manifests a phenotype when grown under high-sucrose conditions, and the null alleles (*cob-4* and *cob-5*) were found to be sterile and lacking

inflorescence stems, in addition to a complete loss of anisotropic growth (Ko, Kim, Jayanty, Howe, & Han, 2006; Roudier et al., 2005).

Furthermore, the lack of a visible phenotype in the root hairs, which extend by tip growth in a cellulose-dependent manner, suggests that *COB* functions only in diffuse growth and not tip growth (Roudier et al., 2005). A further study also found that the expression of the primary cell wall *CESA*s correlated strongly with that of *COB*, strengthening the association between COB and primary cell wall deposition (Persson, Wei, Milne, Page, & Somerville, 2005). Examination of the cellulose in *cob-1* and *cob-4* revealed defects in cellulose deposition in the primary cell wall, and a loss of organized cellulose microfibril orientation (Roudier et al., 2005; Schindelman et al., 2001).

Recent findings have shown that mutations in *MEDIATOR16* (*MED16*), also known as *SENSITIVE-TO-FREEZING6* (*SFR6*), can partially rescue the growth defects in the *cob-6* knock-down mutant. Double-mutant analysis of the *SFR6* knock-out mutant *sfr6-3* and *cob-6* showed a rescue in cellulose levels compared to the *cob-6* single mutant, but no changes in the expression of *cob-6,* suggesting that *sfr6-3* may suppress the cellulose deficiency (Sorek et al., 2015). Cellulose biosynthesis inhibitor assays showed that *cob-6* was hypersensitive to all inhibitors tested while *sfr6-3 cob-6* showed significantly higher resistance, suggesting that *sfr6-3* causes resistance to perturbations in cellulose biosynthesis (Sorek et al., 2015). RNA sequencing (RNAseq) analysis revealed that genes involved in pectin modification were mis-regulated in *cob-6* but not *sfr6-3 cob-6* (Sorek et al., 2015). Pectin methylesterifcation inhibitors (PMEIs) *PMEI18* and *PMEI19* were found to be the most highly mis-regulated, and further analyses showed that over-expression of *PMEI18* and *PMEI19* resulted in partial suppression of the *cob-6* phenotype, suggesting a relation between *COB* and pectin (Sorek et al., 2015).

Localization studies on COB using an antibody specific to the N-terminal region of COB and transmission electron microscopy (TEM) have shown it to be predominantly distributed in the cell wall at varying distances from the plasma membrane, suggesting that the GPI-anchor is cleaved as cells develop, in addition to distribution at the plasma membrane and within the Golgi (Roudier et al., 2005). Furthermore, immunofluorescence showed COB to be localized in a transverse banding pattern in the cell wall (Miki Fujita, Lechner, Barton, Overall, & Wasteneys, 2012; Roudier et al., 2005). Although immunolabeling did not reveal any connection between COB and cortical microtubules, disruption of cortical microtubules using the microtubule destabilizing drug oryzalin resulted in dissipation of COB's transverse banding pattern (Roudier et al., 2005). When combined with the loss of organized cellulose MFs in the *cob-1*and *cob-4* mutants, it was suggested that COB may play a role in the organization of cellulose MFs in a microtubule-dependent manner (Roudier et al., 2005).

1.5.2 COBRA-likes

In Arabidopsis, members of the *COB* gene family have been shown to have some degree of overlap in expression in most plant organs, with *COB* being an outlier with its relatively high expression in most plant organs compared to the *COBLs* (Brady et al., 2007). Exceptions are *COBL10* and *COBL11*, which have been shown to be expressed only in the inflorescence or floral tissue, suggesting that the two may function as a gene pair (Brady et al., 2007; Roudier et al., 2002). Expression of *COBLs* has also been shown to be highly regulated in a developmental-, tissue-, and cell-specific manner. For example, while *COBL4*, *COBL7*, *COBL8*, and *COBL9*, are all expressed in the rosette leaves, they all have very distinct expression patterns: *COBL4* is expressed only in localized areas and in the petiole; *COBL7* and *COBL8* are expressed throughout the vasculature though *COBL8* is expressed in an acropetal manner; and *COBL9* is

expressed only at the bases of the trichomes overlying leaf primary vasculature (Brady et al., 2007).

Like COB, the mechanism of protein function for the COBLs has yet to be elucidated. However, COBLs have also been shown to be important in cell wall deposition during specific developmental stages. Of the 11 COBLs, 5 have been characterized: COBL9 in the elongation of root hairs (Ringli, Baumberger, & Keller, 2005); COBL10 and COBL11 in pollen tube elongation (Sha Li et al., 2013); COBL4 in xylem differentiation (Y. Li et al., 2003; L. Liu et al., 2013); and COBL2 in mucilage secretion (Ben-Tov et al., 2018). The other 6 COBLs have yet to be functionally characterized.

In addition, despite the similar influence on cellulose deposition by COB and the COBLs, and the high degree of homology, there appears to be no functional redundancy between COB and any of the COBLs (Schindelman et al., 2001). Preliminary functional analysis of the COBL family by Sorek et al. (preprint) (2016) showed the inability of *COBL1*, *COBL5, COBL9,* and *COBL11* to complement the *cob* phenotype, suggesting that sequence variation within the *COB* gene family has functional significance.

Of the COBLs, the most well-studied is the rice homolog of CBL4, Brittle Culm1 (BC1). BC1 has been shown to be important in rice secondary cell wall biosynthesis in developing sclerenchyma cells and in vascular bundles (Y. Li et al., 2003). The *bc1-1* and *bc1-2* mutants have altered cell wall compositions, with a severe reduction in cellulosic glucose and hemicellulosic xylose (Y. Li et al., 2003). In addition, it has been shown that BC1 plays an important role in maintaining cellulose microfibril crystallinity, and that changing *BC1* expression or mutating BC1 causes significant changes in cellulose crystallinity (L. Liu et al., 2013). The CBD in BC1 has also been shown to interact specifically with crystalline cellulose

via specific aromatic residues that are essential to binding (L. Liu et al., 2013). The *bc1* mutants with altered residues in the cellulose binding motif show altered cell wall compositions similar to that of *bc1-1* and *bc1-2*, suggesting that BC1 modulates cellulose assembly by interacting with cellulose and affecting microfibril crystallinity (Y. Li et al., 2003; L. Liu et al., 2013).

1.6 Re-visiting the anti-COB antibody and the findings of Roudier et al. (2005)

Current models of cellulose biosynthesis typically place COBRA as a structural component of the plant primary cell wall, predominantly based on the findings of Roudier et al. (2005) using a polyclonal antibody generated against the COB protein. However, recent evidence suggests that the polyclonal antibody generated is, while likely able to recognize COB, able to recognize other members of the *COB* gene family. Furthermore, some of the findings from Roudier et al. (2005) are at odds with more recent bioinformatic and expressions studies.

The polyclonal anti-COB antibody was generated using an 150 amino acid peptide sequence and verified using COB protein isolated from *Escherichia coli* (*E. coli*). A protein BLAST search using the 150 amino acids used to generated the antibody shows that while it has high specificity to COB, there is also high homology to other proteins, namely the COBRA-likes (Table 1.1). This suggests that while the polyclonal antibody is able to recognize COB, it is also extremely likely to recognize other members of the COB gene family.

Gene Name	E Value	Predicted Size (kDa)
COB	3 E-104	51.2
COBL1	1 E-77	50.4
COBL2	1 E-72	49.7
COBL6	6 E-21	51.0
COBL5	7 E-22	22.5
COBL7/SEB1	9 E-14	72.6
COBL10	2 E-11	74.7
COBL11	3 E-11	73.8
COBL8	3 E-10	72.0

Table 1.1. Polyclonal anti-COB antibody is not specific to COBRA

BLAST protein search using the 150 amino acids used to generate the anti-COB antibody (https://blast.ncbi.nlm.nih.gov/). The anti-COB antibody is likely to recognize other members of the COB gene family.

In addition, the anti-COB antibody identified COB as 75 kDa protein that did not show significant changes in size after treatment of *N*-glycosidase or phospholipase C to remove *N*-glycosylation and the GPI-anchor respectively (Roudier et al., 2005). However, un-processed COB is predicted to have a size of 51 kDa, and is estimated to be 48 kDa after post-translational removal of the signal sequence and ω-site. Furthermore, recent findings on the rice *COB* homolog *OsBC1* suggest that the GPI-anchor contributes approximately 15 kDa to the size of BC1 (L. Liu et al., 2013). While there may be differences in rice and Arabidopsis glypiation, this does provide an estimate of 63 kDa for the size of a glypiated COB protein (48 kDa after post-translational modification + 15 kDa GPI-anchor), which is far smaller than the 75 kDa protein identified by (Roudier et al., 2005).

Furthermore, the majority of the of the protein work performed in Roudier et al. (2005) was from callus extracts, but *COB* has been shown to be down-regulated in callus culture and is unlikely to be found in high abundance (Xu et al., 2012). In addition, COBL7/SEB1, which has a predicted size of 72.6 kDa, has been shown to be up-regulated in callus culture making it the likely protein that was recognized by the anti-COB antibody in the Western blots performed in Roudier et al. (2005) (Xu et al., 2012). Furthermore, the protein blots shown in Roudier et al. (2005) suggest that COB is a fairly abundant protein, but attempts to identifying COB using proteomic methods have thus far been unsuccessful (Borner, Lilley, Stevens, & Dupree, 2003; Nühse, Stensballe, Jensen, & Peck, 2004).

1.7 Scientific questions and research objectives

The overall goal of this thesis is to understand the role of COBRA in cellulose deposition in the primary cell wall using the model dicot *Arabidpsis thaliana*. It has been hypothesized that COB's localization to the outer leaflet of the plasma membrane allows it to interact with and/or influence cellulose deposition. COB could interact directly with cellulose microfibrils via its putative CBM as shown in the rice homolog *OsBC1* (L. Liu et al., 2013). Alternatively, COB could indirectly influence cellulose deposition through interaction(s) with the cellulose synthase complex in the plasma membrane. Both of these hypothesis place COB as an integral protein in primary cell wall synthesis by facilitating direct or indirect interactions between the plasma membrane and the cellulose MFs.

In addition, while it has previously been shown that COB can directly or indirectly influence gene transcription through an unknown manner there is no evidence for any COB interacting proteins (Sorek et al., 2015, 2016). As COB is thought to act at the outer leaflet of the plasma membrane, COB interactors may be tightly bound to cell wall polymers and/or the

plasma membrane. Furthermore, abundance is also an issue as COB is not readily detected by proteomic or biochemical methods rendering pull-down assays and functional analyses difficult (Borner et al., 2003).

Furthermore, new findings that cast doubt on the work previously done of COB using an anti-COB antibody demonstrates the need for better tools to examine COB's function. As the previous anti-COB antibody is no longer available, and generation of a new COB-specific antibody is difficult and expensive given the high degree of homology in the COB gene family. In addition, techniques such as live-cell imaging cannot be used using antibodies to label COB. As such, there is a need to move beyond generating an anti-COB antibody and use a different approach to examine COB's function, such as generating COB-fusion reporter constructs.

However, attempts to create COB-fusion reporter constructs has proven to be challenging given the post-translational modifications occurring at both the N- and C-terminus due to removal of the signal sequence and glypiation respectively. Currently there is only a single viable COB-fusion reporter construct, COB-cYFP, with a citrine yellow fluorescent protein (cYFP) inserted at an internal site (Wasteneys lab, unpublished). However, COB-cYFP can only partially complement the *cob-4* null mutant, as measured by its ability to restore anisotropic growth and cellulose content to wild-type levels. This partial rescue thus brings into question the validity of any findings obtained using COB-cYFP. To further explore the role of COB in proper cellulose deposition in the primary cell wall, I had the following objectives:

1. To improve the COB-cYFP lines for live-cell imaging (Chapter 3).

2. To generate a COB-reporter fusion construct that fully complements *cob-4* and to perform biochemical and proteomic analysis (Chapter 4).

3. To search for new potential functional domains in COB (Chapter 5).

For objective 1, the COB-cYFP construct was used as the cloning base to examine if the partial rescue of the construct was due to the known ability for cYFP to self-dimerize by generating a COB-monomeric-cYFP construct (COB-mcYFP). In addition, COB-mcYFP in *cob-4* plant lines were improved upon for live-cell imaging by either crossing the line with the endosomal marker lines wave_2R and wave_129R and by removal of the root hairs through the use of CRISPR/Cas9 technology.

For objective 2, a HisCOB construct was generated and found to be able to fully complement the *cob-4* null mutant. HisCOB was extracted from Arabidopsis *HisCOB/cob-4* seedlings from either a total protein extract prior to purification using immobilized metal ion affinity chromatography (IMAC) or a cell wall protein extract. HisCOB was also sequenced using mass spectrometry after isolation from a total protein extract.

For objective 3, several COB mutants were analyzed in order to determine a protein region of high potential functionality. In addition, COB-fusion constructs that were able to complement *cob-4* were transformed into the wild-type background and their root length and diameter measured. Furthermore, several new mutants were generated in order to examine the functionality of certain COB domains.

Chapter 2: Materials and Methods

2.1 Plant material and growth conditions

The organism used for this study was *Arabidopsis thaliana* (Arabidopsis), Columbia-0 ecotype. The Arabidopsis *cobra-4* (*cob-4*) knock-out T-DNA insertion line used throughout the study was obtained from the Syngenta Arabidopsis Insertion Library (SAIL) collection (SAIL 735D10) (Roudier et al., 2005). Due to seedling lethality of the homozygous *cob-4* mutant, *cob-4* was propagated as heterozygotes by selection using glufosinate (BASTA).

To generate plant lines containing endosomal markers, COB-mcYFP was crossed with the endosomal marker lines wave_129R and wave_2R which correspond to RFP-RabA1g and RFP-RabF2b respectively. Lines containing COB-mcYFP and the desired wave line were identified for containing both cYFP and RFP signal using a Perkin-Elmer UltraView VoX Spinning Disk Confocal microscope. The wave lines were obtained from Niko Geldner (Geldner et al., 2009).

The *hulk-1* point mutants were obtained by obtained by out-crossing the *hulk-1* mutant background from the transgenic COB-HA in *hulk-1* plant line. The COB-HA in *hulk-1* plant line was a generous gift from Georg Seifert.

All seeds were surface sterilized using either chlorine gas or a solution of 10% hydrogen peroxide and 50% ethanol followed by three successive washes in ddH_2O. Seeds were then plated and germinated on Hoagland's medium containing 1.2% Bacto-agar (BD Diagnostics) and no sucrose. If transgenic lines were not homozygous, seeds were grown on Hoagland's medium containing the appropriate antibiotic(s) until antibiotic resistant seedlings could be discerned from non-resistant seedlings (7-14 days). Antibiotics used for this study were kanamycin (50

μg/mL), hygromycin (25 μg/mL) and BASTA (25 μg/uL). The seeds were vernalized for 2-3 days at 4 ºC.

For protein work and live-cell imaging, seeds were germinated and grown in the dark at 21 ºC for 5 days. For sucrose-related protein work, seeds were germinated and grown in the light at 21 ºC for 10 days.

For growth on soil, seeds were transferred to 21 ºC under 24-hours light (full spectrum fluorescence illumination at 75-125 μmol $m^{-2}s^{-1}$) for 7-10 days before being transferred onto soil (Sungro Sunshine Mix 4). Seedlings on soil were grown at 21 ºC in 24-hour light cycles (full spectrum fluorescence illumination at 230 μmol $m^{-2}s^{-1}$).

For induction of sucrose-dependent phenotypes, Hoaglands' media was supplemented with 4.5% sucrose.

2.2 Plant DNA extraction

Plant genomic DNA was extracted from young rosette leaves of *Arabidopsis thaliana.* Two to four young rosette leaves were ground in sucrose solution for immediate use or Edward's solution for long-term storage.

2.2.1 DNA extraction using sucrose solution

Two to four young rosette leaves were ground in sucrose solution (50 mM Tris-HCl; pH 7.5, 300 mM NaCl, and 300 mM sucrose) and boiled for 10 min. The cell debris was pelleted and 1-2 μL of the supernatant used immediately for genotyping.

2.2.2 DNA extraction using Edward's solution

Two to four young rosette leaves were ground or sonicated in Edward's solution (Edwards, Johnstone, & Thompson, 1991), and the cell debris was pelleted. Once the debris was removed, the DNA was precipitated using isopropanol and pelleted. The DNA precipitate was

then washed with 70% EtOH and then allowed to air dry. The DNA precipitate was then re-suspended in ddH_2O and stored at -20 ºC.

2.3 *Escherichia coli* (*E. coli*) chemical transformation

Chemical competent *E. coli* (DH5α) were thawed on ice before use. For a single transformation 50 µL of bacterial suspension was transformed with 3-5 µL of the desired plasmid. The suspension was incubated on ice for 15 min, heat-shocked at 42 ºC for 30 s, and then allowed to recover on ice for 5 min. After recovery, 400 µL of SOB medium (Hanahan, 1983) was added and the suspension incubated at 200 rpm for 1 h at 37 ºC. Following incubation, *E. coli* were cultured on LB agar containing 1.2% agar (BD Diagnostics) plates containing appropriate antibiotics for approximately 16 h at 37 ºC. Independent, resistant colonies were selected and the plasmid isolated. Antibiotics used for this study were ampicillin (100 µg/mL) or kanamycin (50 µg/mL).

2.4 *Agrobacterium tumefaciens* (Agro) chemical transformation

Chemical competent *Agrobacterium tumefaciens* strain GV3101 colonies were thawed on ice before use. For a single transformation 50 µL of bacterial suspension was transformed with about 100 ng of desired plasmid. The suspension was quickly frozen in liquid nitrogen, heat-shocked at 37 ºC for 5 min ,and then allowed to recover on ice for 5 min. After recovery, 400 µL of YEP medium was added and the suspension incubated at 200 rpm for 2 h at 28 ºC. Cultures were then removed from incubation and spread on antibiotic containing YEB agar plates and incubated for 36-48 h at 28 ºC. Independent, resistant colonies were selected for use in Arabidopsis transformation. For Agrobacterium antibiotic selection YEB agar plates contained gentamicin (25 µg/mL) plus either kanamycin (50 µg/mL) or hygromycin (50 µg/mL).

2.5 Bacterial plasmid isolation

Desired bacteria were grown in 5 mL of LB media containing appropriate antibiotics for approximately 18 h at 200 rpm, 37 ºC. The cells were then pelleted at 4500 rpm for 10 min and the supernatant discarded. The pellet was then re-resuspended in cold P1 buffer (50 mM Tris-HCl; pH 8, 10 mM EDTA, 100 µg/mL RNase A (Sigma-Aldrich). P2 buffer (200 mM NaOH, 1% SDS) was then added to the suspension and briefly vortexed, followed by addition of N3 buffer (0.9 M NaOAc, 4.2 M Gu-HCl, and glacial acetic acid (pH 4.8)) and a brief vortex. The suspension was then centrifuged for 10 min at 14,000 rpm and the supernatant transferred to EconoSpin™ DNA Spin Columns (Epoch Life Science) and centrifuged at 14,000 rpm for 1 min. After the flow-through was discarded, the columns were washed twice with PE buffer (10 mM Tris-HCl; pH 7.5, 20 mM NaCl, and 80% EtOH) before allowed to briefly air-dry. Columns were then eluted with ddH_2O.

2.6 COB fusion construct preparation

All constructs were made using either site-directed mutagenesis or Gibson assembly. Colony PCR (cPCR) was performed using Taq DNA polymerase (FroggaBio) to screen for successful bacterial transformants in addition to antibiotic selection before plasmid isolation. Sequencing of constructs was performed using BigDye® Terminator v3.1 (Thermofisher Scientific) by the UBC Nucleic Acid Protein Service Unit. Sequences of primers used for cPCR and sequencing primers can be found in Table 2.1. Bacterial plasmids used for this work were pBluescript KS (-) (pBKS) cloning vector and pCAMBIA2300 binary vector which confer bacterial resistance to ampicillin and kanamycin respectively.

Primer	Sequence (5' to 3')
COBF1131	ATC AGA AGC AGG TCC TCT TGG GAA TG
RP6	GTT CTG TTG GTC CGT CGT TGT AGA
COBF658	TGC ACA TAC TCG CAG TCC CTT
COBF252	CTC CAG GAT GGA CAT TAG GTT GG
COBR760	TGG ATG TCC AAC TTG TGC TTG C
RP4	CAG ACG ATA CGG CGA TGT TAT GG
COBR252	GGT TGG ATT ACA GGT AGG ACC TC

Table 2.1 Primer sequences used for colony PCR and sequencing

2.6.1 Site-directed mutagenesis constructs

Site-directed mutagenesis was performed using Phusion® High-Fidelity DNA Polymerase (NEB) and the appropriate primers. Sequences of primers used for site-directed mutagenesis can be found in Table 2.2.

2.6.1.1 COB-monomeric-cYFP (COB-mcYFP)

Citrine-YFP was excised from COB-cYFP in pBKS plasmid using SacI and XmaI restriction enzymes and ligated into an empty pBKS plasmid also cut by SacI and XmaI (cYFP in pBKS). The cYFP in pBKS plasmid was transformed into *E. coli* and isolated. Site-directed mutagenesis of cYFP in pBKS was performed using primers A206KF and A206KR. The solution was digested with DpnI before being transformed into *E. coli* and the plasmid isolated (mcYFP in pBKS). The cYFP in COB-cYFP was then excised and re-ligated with mcYFP using the restriction enzymes SacI and XmaI to form COB-mcYFP in pBKS. Primers used for cPCR were COBF1131 and RP6, and the sequencing primer used was COBF658.

2.6.1.2 COB-6xHistidine (COB-His)

COB-cYFP in pBKS was used as a template for a modified site-directed mutagenesis reaction using primers HIS1F and XbaIRev in order to generate a COB fragment containing a 6x

His-tag instead of cYFP. The 6x His-containing fragment and COB-cYFP in pBKS were both digested with XbaI and SacI. The cYFP was excised from COB-cYFP in pBKS to leave COB in pBKS, and the 6x-His fragment was ligated into this vector to form COB-His in pBKS. COB-His in pBKS was then transformed into *E. coli* and the plasmid isolated. Primers used for cPCR were COBF1131 and RP6, and the sequencing primer used was COBF658.

Primer	Sequence (5' to 3')
A206KF	GTT GGG GTC TTT GCT CAG CTT GGA CTG GTA GCT CAG GTA G
A206KR	CTA CCT GAG CTA CCA GTC CAA GCT GAG CAA AGA CCC CAA C
HIS1F	ATC GTC GAC CCT GGA GCT GGA GCT CAC CAC CAC CAC CAC CAC GCT GCT GGT GGT GGT CCA CCA ACA AAG AAA GGA ACG
XbaIRev	GAT TCT AGA TTA GGC AGA GAA GAA GAA GAA AAA GAC AAG AAG AGG GAG GAG CAC GGC GGC G

Table 2.2 Primer sequences used for site-directed mutagenesis

2.6.2 Gibson assembly constructs

These constructs were all made utilizing the Gibson assembly cloning protocol (Gibson et al., 2009). Gibson fragments were amplified using Phusion® High-Fidelity DNA Polymerase (NEB) and assembled using Gibson Assembly® Master Mix (NEB). Sequences of Gibson primers used can be found in Table 2.3.

2.6.2.1 6x-Histidine-COB (HisCOB)

COB-His in pBKS was used as a template and amplified using primers GA6HF and GA6HR to generate a 6x-His insert fragment. COB in pBKS was digested with Tth111. The 6xHis insert fragment was assembled with the Tth111 digested COB in pBKS linear plasmid in a 1:3 molar ratio respectively using Gibson assembly to generate HisCOB in pBKS. HisCOB in pBKS was then transformed into *E. coli* and the plasmid isolated. Primers used for cPCR were COBF252 and COBR760, and the sequencing primer used was COBF252.

2.6.2.2 35S*pro*::*COB-mcYFP*

The 35S*pro* region was amplified out of 35S*pro*::*CBD-HA* in pBKS using primers 35S*pro*-CA and 35S*pro*-CD to generate Gibson fragment #1. COB-mcYFP in pBKS was amplified using the primer pair 35S*pro*-CC and 35S*pro*-CF in addition to 35S*pro*-CB and 35S*pro*-CE to generate Gibson fragments #2 and #3 respectively. The three fragments were assembled in a 1:1:1 molar ratio using Gibson assembly to generate 35S*pro*::*COB-mcYFP* in pBKS. 35S*pro*::*COB-mcYFP* in pBKS was then transformed into *E. coli* and the plasmid isolated. Primers used for cPCR were COBF252 and COBR760, and the sequencing primer used was M13 Reverse (-27).

2.6.2.3 COB-mcYFP cellulose-binding domain mutants (W86A and Y60A)

COB-mcYFP in pBKS was used as the template for generation of all the Gibson fragments. Four Gibson fragments were generated using the following four primer pairs: CBDA and CBDE; CBDB and CBDFa/CBDFb; CBDCa/CBDCb and CBDG; and CBDD and CBDH. The a and b denote primers specific for generating the amino acid substitutions W86A and Y60A respectively. The four fragments were assembled in a 1:1:1:1 molar ratio using Gibson assembly to generate W86A *COB-mcYFP* in pBKS and Y60A *COB-mcYFP* in pBKS. These constructs were then transformed into *E. coli* and the plasmids isolated. Primers used for cPCR were COBF252 and RP4, and the sequencing primers used were COBR252 and COBF658.

Primer	Sequence (5' to 3')
GA6HF	GGT CCC AAG AAA CTT CAC TCT CAT GGG ACC TGC TGG AGG TGG AGC TCA TC
GA6HR	TTT GCT GGA CCA CAA GTG TAA CCT GGA CCA GGA CCA CCA CCA GCA GCG TG
35S*pro*:CA	GGG ACC AAA AGC TGG GTA CCT CGA CGA ATT AAT TCC AAT C
35S*pro*:CD	CTG GAG AAG AAA GAC TCC ATC GTG TCC TCT CCA AAT GAA A
35S*pro*:CC	TTT CAT TTG GAG AGG ACA CGA TGG AGT CTT TCT TCT CCA G
35S*pro*:CF	TAT AGG GCG AAT TGG AGC TCT CTA GAT TAG GCA GAG AAG A
35S*pro*:CB	GAT TGG AAT TAA TTC GTC CAG GTA CCC AGC TTT TGT TCC C
35S*pro*:CE	TCT TCT CTG CCT AAT CTA GAG AGC TCC AAT TCG CCC TAT A
CBDA	TCA TGT ACG AGT GTG GTG AGC TCC AAT TCG CCC TAT AGT G
CBDE	AAT CAG TCA AAT CTT AAG GTA CCC AGC TTT TGT TCC CTT T
CBDB	AAA GGG AAC AAA AGC TGG GTA CCT TAA GAT TTG ACT GAT T
CBDFa	CAT ATA ACT TCC TTC TTT GCC GCT TTC CAA CCT AAT GTC CAT C
CBDFb	CAG GTT CTT GAA CTT ACA ACA GCG CCA TCA GGA GTC CAG CTC A
CBDCa	GAT GGA CAT TAG GTT GGA AAG CGG CAA AGA AGG AAG TTA TAT G
CBDCb	TGA GCT GGA CTC CTG ATG GCG CTG TTG TAA GTT CAA GAA CCT G
CBDG	CAA AAC CGT AAA TCC GAG ATT CTA GAT TAG GCA GAG AAG A
CBDD	TCT TCT CTG CCT AAT CTA GAA TCT CGG ATT TAC GGT TTT G
CBDH	CAC TAT AGG GCG AAT TGG AGC TCA CCA CAC TCG TAC ATG A

Table 2.3 Primer sequences used for Gibson assembly

Row colors denote primer pairs. The a and b denote primers specific for W86A and Y60A constructs respectively.

2.6.3 Cloning into binary vector

All constructs made in pBKS were excised and ligated into the binary vector pCAMBIA2300 (pCA2300). For cYFP-containing constructs, desired construct and empty binary vector were digested using KpnI and SacI and ligated. For 6x-His-containing constructs, desired construct and empty binary vector were digested using KpnI and PmlI and ligated. Constructs were then transformed into *E. coli* and the plasmids isolated. Primers used for cPCR were the same as those used for cloning into pBKS.

2.7 *CAPRICE* CRISPR/Cas9

The egg cell-specific promoter driven CRISPR/Cas9 molecular toolkit for Arabidopsis was a gift from Qi-Jun Chen (Wang et al., 2015). The two gDNAs used to knock-out *CAPRICE* were selected for using the CHOPCHOP web tool for genome editing (Montague, Cruz, Gagnon, Church, & Valen, 2014). Generation of CRISPR/Cas9 constructs was performed aas described by Xing et al. (2014). Primer sequences used for CRISPR/Cas9 construct generation can be found in Table 2.4.

Primer	Sequence (5' to 3')
CPC DT1-BsF	ATA TAT GGT CTC GAT TGA TGT TTC GTT CAG ACA AGG GTT
CPC DT1-F0	TGA TGT TTC GTT CAG ACA AGG GTT TTA GAG CTA GAA ATA GC
CPC DT2-BsR	ATT ATT GGT CTC GAA ACG CGA TCA ACT CCC ACC TAC C
CPC DT2-R0	AAC GCG ATC AAC TCC CAC CTA CCA ATC TCT TAG TCG ACT CTA C

Table 2.4. Primer sequences used for CRISPR/Cas9

2.8 Transforming *Arabidopsis thaliana*

Antibiotic-resistant *Agrobacterium tumefaciens* transformed with the desired vector were selected and cultured in liquid YEB medium containing kanamycin (50 µg/mL) and gentamycin (25 µg/mL) for 40 h at 200 rpm at 28 ºC. After 40 h, cultures were transferred to fresh liquid YEB media and incubated for 6-8 h at 200 rpm at 28 ºC. Approximately 3-4 week old Arabidopsis plants were trimmed of mature flowers and developing siliques. Silwet® L-77 (*Phyto*Technology Laboratories) was added to the cultures and trimmed Arabidopsis plants were dipped using the floral dip method (Clough & Bent, 2008). Plants were allowed to rest in the dark at room temperature overnight in a humid space before being returned to growth chambers.

2.9 Segregation and Selection of Transformed Plant Lines

Seeds from floral-dipped plants (T0 generation) were selected for by germination on media containing appropriate antibiotic(s). At least 15 antibiotic resistant seedlings from the T0 generation were grown and the seeds harvested to produce the T1 generation. T1 seedlings were screened for single-copy transformants via germination on media containing appropriate antibiotic(s). T1 lines exhibiting a 3:1 ratio of resistant:non-resistant, indicative of a single copy transformant, were further segregated for homozygosity of both the transformed construct and the desired plant background in the T2 and/or T3 generations. Homozygosity of the transformed construct was determined when all seedlings from a given line were resistant to the appropriate antibiotic. Homozygosity of the transformed background was determined when all seedlings were susceptible or resistant to BASTA for wild-type and *cob-4* backgrounds respectively.

Construct phenotypes were determined by comparison of homozygous T3 or T4 seedlings from at least 3 different initial T0 lines.

2.10 Plant growth measurements

Five-day-old light-grown Arabidopsis seedlings were used for all plant growth measurements. Seedlings were scanned using a CanoScan 8800F (Canon) scanner and measurements done in Fiji (Schindelin et al., 2012). Root length was measured using the NeuronJ plug-in (Meijering et al., 2004). Tracings were made between the root tip and the bottom of the hypocotyl and the length quantified. Root diameter was measured as the width of the most representative region of the root.

Statistical analyses were performed using the GraphPad™ Prism® software.

2.11 Cellulosic glucose assay

Cellulosic glucose was measured using gas-chromatography mass spectrometry (GC-MS). Ten-day-old light-grown Arabidopsis seedlings were quickly frozen in liquid nitrogen and freeze-dried before sample preparation. Sample processing and analysis of cell wall polysaccharides was performed by our collaborator Charles Hocart (Australian National University) as previously described by Lane et al. (2001).

2.12 Cell wall protein extraction

Cell wall proteins were extracted from 5-day-old dark-grown seedlings using a protocol modified from Feiz et al. (2006). Approximately 7 g of tissue were ground in 5 mL of Sol A (0.4 M sucrose and 5 mM acetate buffer, pH 4.6), 50 µL of plant protease inhibitor cocktail (Sigma-Aldrich), and 0.5 g PVPP. The homogenized tissue was vortexed for 30 min at 4 ºC before being centrifuged for 15 min at 1000 g at 4 ºC. The supernatant was discarded and the residue re-suspended in 500 µL of Sol B (0.6 M sucrose and 5 mM acetate buffer, pH 4.6) before being centrifuged for 15 min at 1000 g at 4 ºC. The supernatant was discarded and the residue re-suspended in 500 µL of Sol C (1 M sucrose and 5 mM acetate buffer, pH 4.6) and centrifuged for 15 min at 1000 g at 4 ºC. The supernatant was discarded and the residue transferred to 40 µM nylon cell strainers (BD Falcon^{TM}) and thoroughly washed with 5 mM acetate buffer, pH 4.6. The residue was then centrifuged for 15 min at 1000 g at 4 ºC and the supernatant decanted. The residue was re-suspended in 100 µL of Sol D (0.2 M $CaCl_2$ and 5 mM acetate buffer, pH 4.6) and 3 µL of plant protease inhibitor cocktail and vortexed for 5-10 min at room temperature before being centrifuged for 15 min at 4000 g at 4 ºC. The supernatant was retained as the $CaCl_2$ fraction. The residue was re-suspended in 100 µL of Sol E (2 M LiCl and 5 mM acetate buffer, pH 4.6) and 3 µL of plant protease inhibitor cocktail and vortexed for 5-10 min at room

temperature before being centrifuged for 15 min at 4000 g at 4 ºC. The supernatant was retained as the LiCl fraction and the residue discarded.

2.13 Purification of HisCOB using immobilized metal ion affinity chromatography

2.13.1 Total protein extraction

Total protein was extracted from 5-day-old dark-grown seedlings. For protein extraction from treated seedlings, seedlings were incubated for 1 h in the dark at room temperature in the appropriate solution (ddH_2O, 0.8 M mannitol, or 0.1% DMSO). Approximately 3-5 g of tissue was ground in 9-15 mL of homogenization buffer (150 mM NaCl, 1 mM EDTA, 0.5% Triton X-100, and 50 mM Tris-HCl, pH 7.5) containing protease inhibitor (10 µL of plant protease inhibitor cocktail (Sigma-Aldrich) per 10 mL of buffer) using a cold mortar and pestle. The homogenized tissue was centrifuged for 20 min at 15,000 g at 4 ºC. The supernatant was decanted and centrifuged again for 20 min at 15,000 g at 4 ºC to remove any residual plant debris.

2.13.2 Immobilized metal ion affinity chromatography

His-tagged protein was isolated using Ni-NTA Agarose (Qiagen) under native and denaturing conditions. Approximately 2-3 mL of resin in a gravity-flow column was used for each extraction. Immobilized metal affinity chromatography was performed as described in the HisPur™ Ni-NTA resin (ThermoFisher) manual. For denaturing conditions, an extra 1 h incubation at 4 ºC, rotating, step was added after addition of equilibration buffer with total protein extract.

2.14 Protein precipitation using Trichloroacetic Acid (TCA)

Eluted protein solution was mixed with 100% TCA until a 20% TCA solution was reached. This 20% TCA solution was thoroughly vortexed and incubated overnight at -20 ºC.

The solution was then centrifuged at 15 500 rpm for 15 min at 4 ºC and the supernatant decanted. The resulting pellet was then rinsed 2 times with 90% ice-cold acetone and the residual acetone left to evaporate. The pellet was then re-suspended in 1% SDS in 0.1x PBS and 5x Laemmeli sample buffer and run on a 12% SDS-PAGE gel.

2.15 Western blot

PVDF membrane with transferred proteins were blocked for 1 h at RT with 5% BSA in TBST. After blocking, membranes were washed 3x with TBST for 5-10 min. Primary antibodies (1:2000 mouse anti-His (Sigma-Aldrich) or 1:5000 mouse anti-GFP (Roche)) in 5% BSA in TBST was added and membranes were incubated overnight at 4 ºC. Membranes were then washed 3x with TBST for 5-10 min and incubated with secondary antibody (1:5000 anti-mouse HRP (Cell Signaling Technologies) in 5% BSA in TBST for 1 h at room temperature. Membranes were washed 3x with TBST for 5-10 min and 1x with TBS for 5-10 min before being incubated for 1 min with Pierce™ Western Blotting Substrate then imaged.

2.16 Protein mass spectrometry

Protein bands on SDS PAGE were visualized as described by Candiano et al. (2004). In-gel digest of the desired protein band(s) was performed as described by Shevchenko et al. (1996). Running of the LC-MS/MS and analysis of the mass spectrometry data was performed by our collaborator Jenny Moon (Foster lab, UBC).

Chapter 3: Improvement of COB-cYFP for Live-cell Imaging

3.1 Introduction

COBRA (COB) is a GPI-anchored protein that has been previously shown to be involved in cellulose biosynthesis in primary cell walls (Roudier et al., 2005; Schindelman et al., 2001). The *cob* mutants typically exhibit a loss of growth anisotropy and perturbations in cellulose crystallinity and content. For example, the *cob-1* point mutant exhibits conditional radial swelling and a reduction in cellulosic glucose and cellulose crystallinity when grown on sucrose-containing media while the *cob-4* null mutant is seedling lethal, suggesting the COB is essential for proper synthesis and/or deposition of cellulose in the primary cell wall (Roudier et al., 2005; Schindelman et al., 2001). Furthermore, COB has been shown to be highly co-expressed with the cellulose synthases (CESAs) involved in primary cell wall biosynthesis, and with proteins that can directly interact with the cellulose synthase complex (CSC) such as KORRIGAN (Vain et al., 2014), CMU1 and 2 (Z. Liu et al., 2016), and CSI1/POM2 (Gu et al., 2010; Persson et al., 2005).

Despite the clear relationship between COB and cellulose biosynthesis, it is still unknown how COB can modulate cellulose or if COB can directly interact with the CSC. A large portion of this uncertainty stems from the fact that generation of COB reporter fusion constructs has proven to be challenging. As COB undergoes posttranslational modifications at the N- and C-termini, via removal of the signal peptide and glypiation respectively, and the presence of a putative cellulose binding domain, traditional methods of generating a reporter fusion construct by fusing reporter tags to the N- or C-termini are unviable (Figure 3.1). As such, previous attempts at generating COB-fusion constructs have involved inserting tags at internal regions of the COB protein to mixed success (Table 3.1). An added challenge in inserting tags at an internal

region is the high degree of homology found in the COB gene family, suggesting high degrees of functional or structural importance in the conserved amino acids (Figure 3.2).

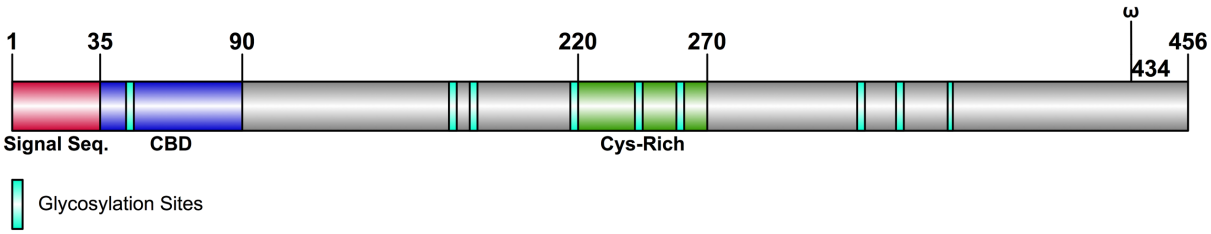

Figure 3.1. Schematic of the COBRA protein (51 kDa)

COBRA (COB) contains an N-terminal signal sequence and a C-terminal glypiation site. COB also contains a putative cellulose binding domain and a cysteine rich domain. CBD = cellulose-binding domain, ω = glypiation site.

Tag	Insertion Site	Rescue *cob-4* Lethality?	Phenotype
FlAsh	N-terminal	No	N/A
mCherry	N-terminal	No	N/A
mCherry	Internal (a.a. 274)	No	N/A
paGFP	Internal (a.a. 278)	No	N/A
TagRFP	Internal (a.a. 278)	Yes	Dwarf, severe radial swelling
HA	Internal (a.a. 428)	Yes	Dwarf, radial swelling
cYFP	Internal (a.a. 278)	Yes	Dwarf, radial swelling

Table 3.1. Currently known COB-fusion constructs

Attempts to create functional COB-fusion constructs have been met with mixed success. While both COB-TagRFP and COB-cYFP can both complement *cob-4* lethality, COB-TagRFP had a much more severe phenotype than COB-cYFP and was no longer used.

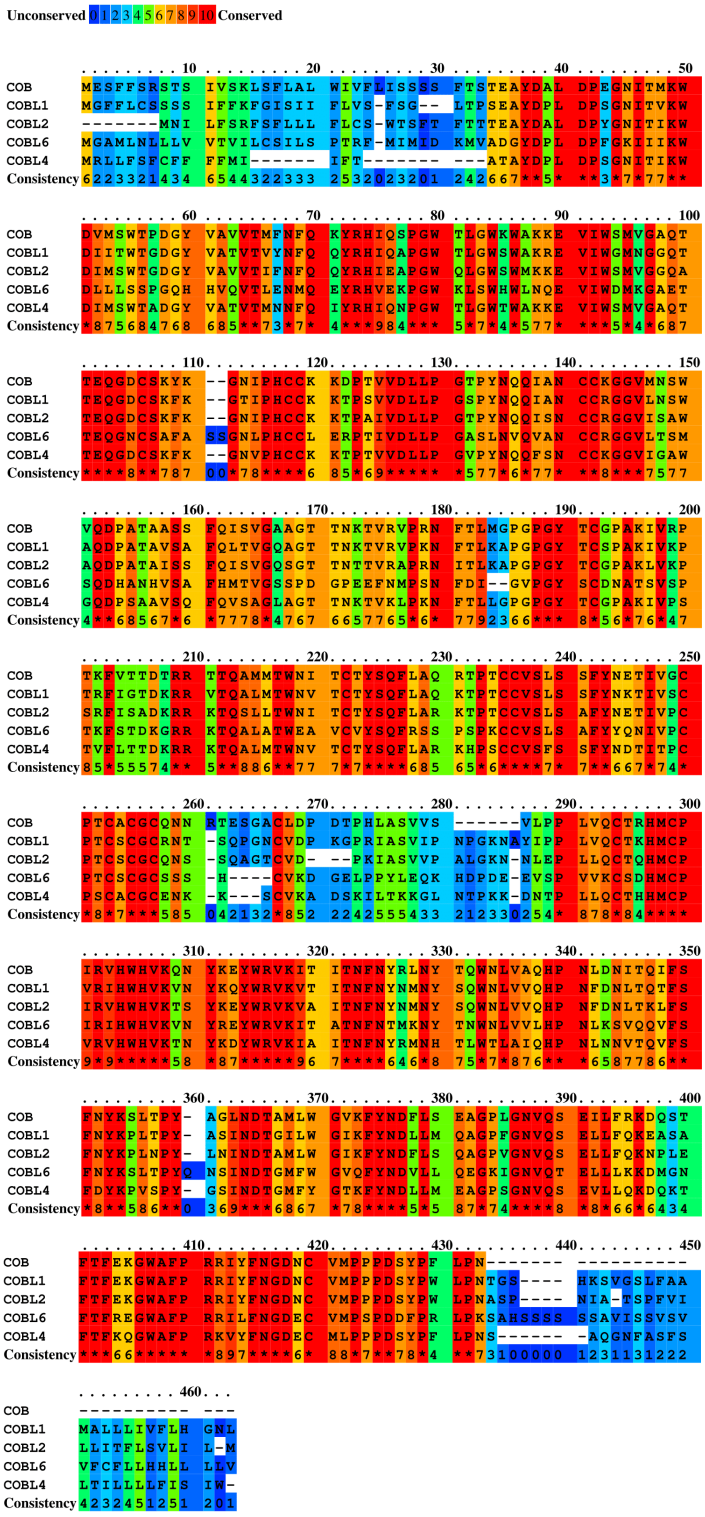

Figure 3.2. Amino acid homology of COBRA and the type I COBRA-likes

COB and the single cellulose binding domain COBLs share a high degree of homology. Conservation scoring obtained using PRALINE (Simossis and Heringa, 2005).

In spite of these difficulties, a native promoter driven COB-citrine-YFP (COB-cYFP) fusion construct generated in the Wasteneys lab has been reported to be able to complement the *cob-4* null mutant. However, while COB-cYFP is able to rescue the seedling lethality of *cob-4*, it still exhibited a constitutive radial swelling and a reduction in root length phenotype suggesting that the COB-cYFP protein was not fully functional. This reduction in functionality may have been caused by the known ability for cYFP to self-dimerize or the relatively large size of cYFP compared to that of the native COB protein, 27 kDa (Day & Davidson, 2009) and 51 kDa respectively.

Another flaw of the COB-cYFP construct is the difficulty in applying drug treatments and stains during live-cell imaging. Live-cell imaging of COB-cYFP has been done solely in dark-grown hypocotyls, as the presence of root hairs in the root led to complications in imaging. However, hypocotyls are fairly recalcitrant to drug treatments and stains compared to roots due to the cuticle. The ability to remove or reduce the presence of root hairs would thus be a boon in imaging COB-cYFP. In addition, preliminary findings using COB-cYFP suggest that COB also undergoes endocytosis, but it is currently not possible to differentiate COB-cYFP that is newly synthesized and being secreted from those that are endocytosed.

Furthermore, it is not known if COB functions as a distinct monomer, or if its function is dependent on interaction with other proteins. Given its apoplastic and cell wall localization in addition to its importance in cellulose biosynthesis it has been hypothesized that COB may function as part of the CSC and be able to physically interact with the CESAs (Roudier et al., 2005). However, identification of components of the heteromultimeric cellulose synthase complex has proven to be challenging due to the difficulties in purifying intact, active CSCs

(Guerriero, Fugelstad, & Bulone, 2010). Preliminary findings by Sorek et al. (preprint) (2016) using a membrane based yeast two-hybrid screen failed to identify any positive COB interactors.

As COB has been implicated to be involved with the transcriptional co-activator MEDIATOR complex, whose individual subunits can be localized to the cytosol (Mauldin et al., 2013; Sorek et al., 2015; Yin & Wang, 2014). As COB appears to in the secretion pathway when it is intercellular, it seems unfeasible that COB can interact with cytosolic proteins. Identification of COB interactors using pull-down assays has also proven to be challenging as COB cannot be readily detected using proteomic methods (Borner et al., 2003; Nühse et al., 2004). This suggests that COB is at low abundance under native conditions. As Roudier et al. (2005) had previously reported the ability of a constitutive over-expression Cauliflower mosaic virus 35S promoter (35S) driven COB cDNA to rescue the *cob-4* null mutant, it may be possible to drive tagged-COB expression using 35S in order to overcome the abundance issues for proteomic analysis. However, the ability for 35S*pro*::COB to rescue *cob-4* is surprising as cellulose synthesis is known to be tightly regulated and, given the relationship between cellulose biosynthesis and COB, constitutive COB expression would be expected to be detrimental.

The primary objectives of this chapter were to improve upon the COB-cYFP construct for live-cell imaging and for biochemical work. This was accomplished by generating a version of COB-cYFP (COB-mcYFP) where the cYFP could no longer self-dimerize, and by optimizing COB-mcYFP in *cob-4* plant lines for specific live-cell imaging experiments.

3.2 Results

3.2.1 COB-monomeric-cYFP better complements *cob-4*

Since COB-dimeric-cYFP (COB-dcYFP) had a relatively severe phenotype that may have been caused by the dimerization of cYFP, the amino acid substitution A206K was

performed in cYFP using site-directed mutagenesis (Figure 3.3A). COB-monomeric-cYFP (COB-mcYFP) was found to better complement the *cob-4* null mutant (Figure 3.3A). Quantification of root length and diameter shows a complete rescue of the radial swelling seen in COB-dcYFP, in addition to an increase in root length, though not to wild-type levels (Figure 3.3B,C). Analysis of cell wall polysaccharides shows that COB-mcYFP is able to restore *cob-4* cellulosic glucose back to wild-type levels, while there is a reduction in cellulosic glucose in COB-dcYFP (Figure. 3.3D). These findings demonstrate that fluorophore dimerization can interfere with a protein's native function, as COB-mcYFP shows significantly better rescue of *cob-4* than COB-dcYFP. Thus COB-mcYFP functions as a better COB reporter line for live-cell imaging.

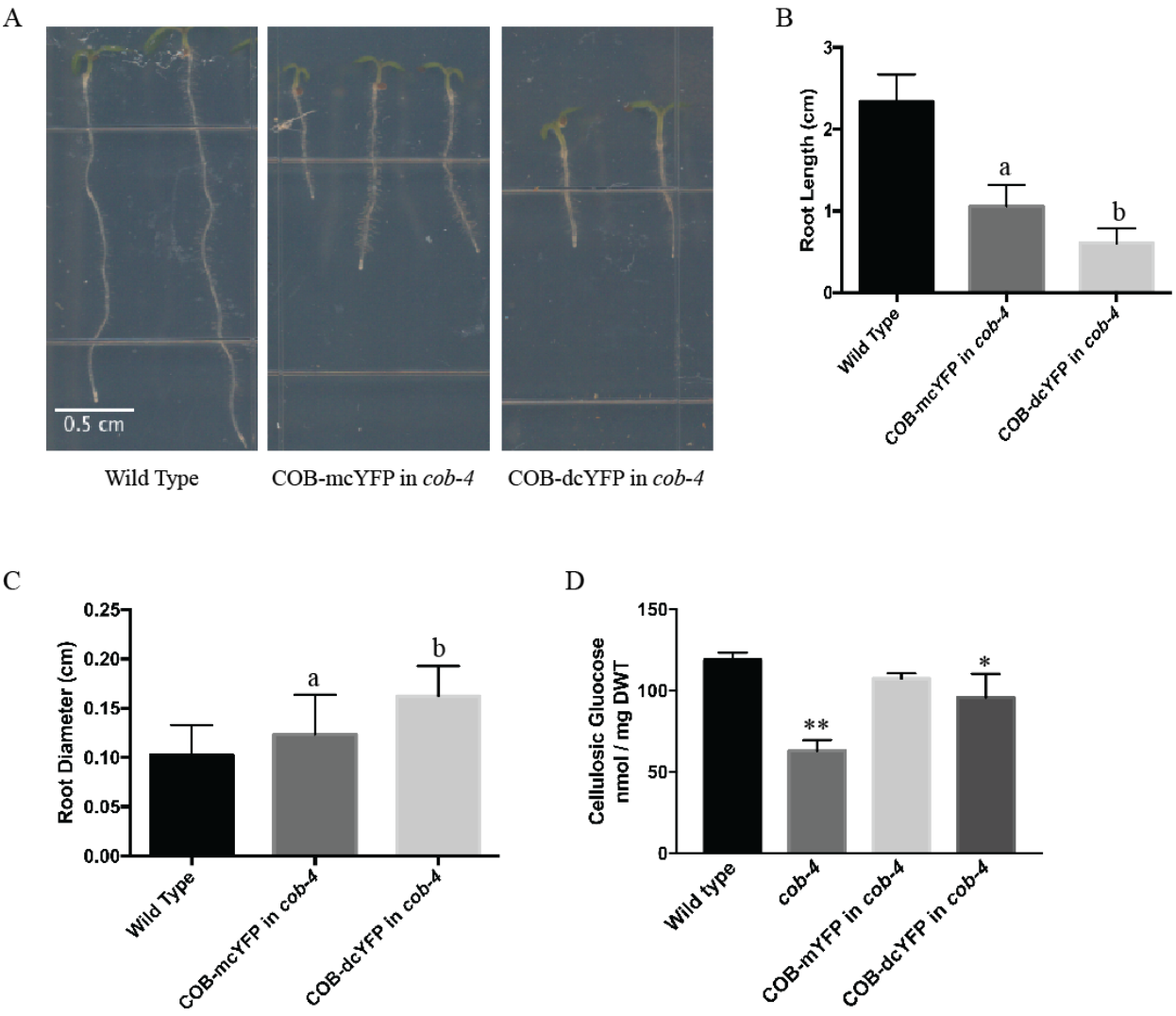

Figure 3.3. COB-monomeric-cYFP is able to better rescue *cob-4*

A) Five-day-old seedlings. COB-mcYFP is able to complement *cob-4* better than COB-dcYFP as shown by their longer roots and decrease in radial swelling. Phenotypes were determined from at least three individually transformed lines. (B, C) Root length (B) and diameter (C) of five-day-old seedlings shows that COB-mcYFP is a stronger complement of *cob-4* than COB-dcYFP. Values are mean ± S.E., N > 35. Letters denote statistical differences between groups (Tukey's test, $p < 0.05$). (D) Cellulose level is restored to wild-type levels in COB-mcYFP, but not in COB-dcYFP transgenic plants. Asterisks denote statistical differences compared to wild-type (Tukey's test, * = $p < 0.05$, ** = $p < 0.0001$). Values are mean ± S.E. from more than 3 biological replicates and 2 technical replicates. DWT = dry weight tissue.

3.2.2 CRISPR/Cas9 *CAPRICE* knock-outs have reduced root hairs

In order to generate a imaging system for COB-mcYFP that is more amenable to drug treatments and stains, *caprice* (*cpc)* knock-outs were generated in COB-mcYFP in *cob-4* seedlings using CRISPR./Cas9. As *CAPRICE* has previously been shown to promote the differentiation of the trichoblasts that form root hairs, *caprice* knock-outs should show a severe reduction in the number of root hairs allowing for easier imaging of the root (Wada et al., 2002). Screening of the successfully transformed T1 seedlings yielded one that had a significant reduction in the amount of root hairs when viewed under a dissecting scope. Currently the successful COB-mcYFP in *cob-4/cpc* line is being propagated.

3.2.3 COB-mcYFP crossed with endosomal markers

In order to discern if the COB-mcYFP puncta seen in live-cell imaging were exocytic or endocytic, COB-mcYFP in *cob-4* was crossed with the Wave endosomal marker lines 129R and 2R which correspond to RFP-RabA1g and RFP-RabF2b respectively (Geldner et al., 2009). Preliminary screening of the F1 lines for fluorescence in both fluorophores showed poor signal in all RFP-RabA1g containing seedlings, and usage of this line was discontinued. Seedlings containing strong signal in the COB-mcYFP in *cob-4* x wave_2R F1 line were further propagated.

3.2.4 COB-mcYFP is not detected in the cell wall

Though it was previously found that COB-dcYFP could not be detected in the cell wall, those cell wall extracts were performed using the dimeric-cYFP construct and not the monomeric version, and given that COB seems to be in low abundance according to proteomic data, a concentration step may be needed in order to isolate enough protein for visualization on a Western blot. As such, cell wall protein extracts were performed using COB-mcYFP and the

protein extracts concentrated via precipitation before immunoblotted using an anti-GFP antibody.

However, there was no detectable COB-mcYFP in either the $CaCl_2$ or LiCl fractions even after precipitation of the cell wall protein extracts (Figure 3.4). It is unlikely that COB-mcYFP is unable to be secreted into the apoplast as it is still able to partially complement *cob-4*, but its inability to fully complement the null mutant may be caused by mcYFP interfering with COB's rate of secretion. Alternatively, COB-mcYFP may be in such low abundance that it is not visible on a Western blot even after a precipitation step.

Lipid transfer protein G (LTPG) -cYFP (53 kDa) was used as a positive control, and was readily found both the $CaCl_2$ and LiCl fractions. The 25 kDa bands are likely loose cYFP, potentially caused by the extraction and precipitation process. It is likely that overloading of protein extracts from LTPG-cYFP has caused bleed-through of protein to other lanes.

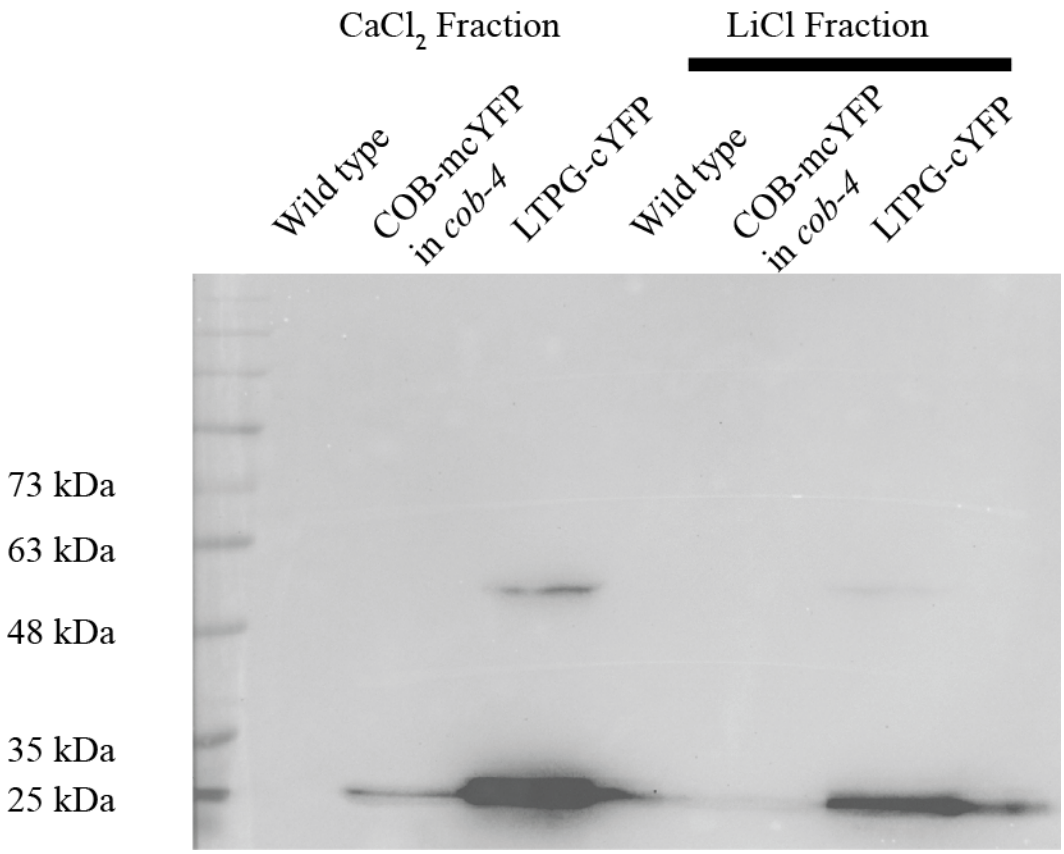

Figure 3.4. Immunoblot of COB-mcYFP cell wall protein extracts

Immunoblot of cell wall protein extracts from wild-type, HisCOB in *cob-4*, and LTPG-cYFP seedlings using anti-GFP antibody. $CaCl_2$ and LiCl fractions represent pectin-associated proteins and cellulose-associated proteins respectively. No bands corresponding to COB-mcYFP are visible from the cell wall extracts. Wild type and LTPG-cYFP were used as negative and positive control respectively. The 53 kDa bands visible in both $CaCl_2$ and LiCl fractions of LTPG-cYFP represent full-length protein. The 25 kDa bands are likely loose cYFP, potentially caused by the extraction and precipitation process. It is likely that overloading of protein extracts from LTPG-cYFP has caused bleed-through of protein to other lanes. Visible bands were present only when the eluate underwent a 20-fold precipitation/concentration step, indicating low cellular abundance.

3.2.5 Over-expression of COB-mcYFP cannot complement *cob-4*

Given the difficulties in extracting enough COB protein for proteomic analysis, it appears that there is low relative expression of COB in root tissues (Borner et al., 2003; Nühse et al., 2004). As 35S*pro*::COB was previously reported to complement *cob-4*, a 35S*pro*::COB-mcYFP construct could allow isolation of enough protein for proteomic analysis and for screening of

protein-protein interactions. However, 35S*pro*::COB-mcYFP caused developmental defects in the T1 generation immediately after transformation. Many of the T1 lines had a reduction in inflorescence stem length and siliques that were aborted early on after fertilization, suggesting sterility; the nature of this sterility remains to be determined. Out of 20 T1 seedlings that were transplanted to soil, only 5 were able to produce seeds. Of the few T1 lines that were able to produce seeds, segregation in the T3 and T4 generations yielded no lines homozygous for both 35S*pro*::COB-mcYFP and *cob-4*, indicating a failure of 35S*pro:*COB-mcYFP to complement *cob-4*.

3.3 Discussion

3.3.1 The importance of tag choice in reporter fusion constructs

While it was previously established that COB-dcYFP is able to complement the *cob-4* null mutant, albeit partially, that insertion site does not amenable to other fluorophores as evidenced by the poor rescue of the paGFP and tagRFP constructs (Table 3.1). Despite the similar overall structure of the three fluorophores, the subtle differences between them rendered the paGFP and tag-RFP constructs non-viable.

In addition, I have demonstrated that the ability of cYFP to form a heterodimer can severely impact the function of a construct, as COB-mcYFP shows a significantly stronger rescue compared to the COB-dcYFP. Furthermore, much of the literature does not specify on the usage of “dimeric” versus “monomeric” cYFP in the generation of recombinant protein constructs, which can drastically change the viability of the construct. In addition, the rather severe phenotype that can be attributed to the dimerization of cYFP also brings into question the findings obtained from constructs utilizing “dimeric” cYFP.

However, COB-mcYFP is still unable to fully complement *cob-4* as the seedlings still have a slight radial swelling phenotype. This is likely due to the large relative size of mcYFP compared to that of the COBRA protein (27 kDa vs 51 kDa respectively) which may interfere with proper folding of the protein and interfere with protein-protein interactions. As such there is still a need to generate a COB reporter fusion construct that is able to fully complement *cob-4*, likely using non-fluorophore tags such as 6xHis, Myc, HA or FLAG as they are much smaller in size and thus less likely to interfere with protein folding or protein-protein interactions.

3.3.2 The inability for 35S*pro*::*COB-mcYFP* to complement *cob-4*

As previously discussed, one of the major complications in elucidating COB's function is the difficulty in detecting it using proteomic and biochemical methods (Borner et al., 2003; Nühse et al., 2004). Furthermore, COB*pro*::COB-mcYFP was undetectable in the cell wall fraction even after a 20-fold precipitation, suggesting that either secretion is inhibited or compromised by the addition of mcYFP, or that COB-mcYFP is present at undetectable levels even after precipitation. In order to examine if abundance was the main issue, the native COB promoter was replaced with the Cauliflower Mosaic Virus 35S promoter, as 35S*pro*::COB (cDNA) was previously reported to be able to fully complement *cob-4* (Roudier et al., 2005).

However, 35S*pro*::COB-mcYFP in *cob-4* lines were unable to be obtained due to severe developmental defects present even in the initial T1 lines. The lines that were able to propagated were unable to yield plant lines homozygous for 35S*pro*::COB-mcYFP in *cob-4* suggesting that over-expression of COB-mcYFP is unable to complement *cob-4*. This is surprising given that both 35S*pro*::COB and COB-mcYFP have been reported to complement *cob-4* independently. The inability for 35S*pro*::COB-mcYFP to complement *cob-4* suggests that constitutive over-expression of COB causes developmental defects, or that is it addition of mcYFP that is causing

the developmental defects by interfering with protein-protein interactions. At this time however, there are no reports of proteins that interact with COB or that COB plays an important developmental role outside of the root, and it should be noted that while it is reported by Roudier et al. (2005) that 35S*pro*::COB was able to complement *cob-4,* no actual experimental was shown.

As such, alternative approaches to isolate COB for biochemical and proteomic analyses is needed. As bulk isolation of proteins through immunoprecipitation is often not cost-efficient, conjugation of COB with tags such as Myc, FLAG, and HA, which require antibodies for purification, is likely not a realistic approach. However, tags such as the 6xHis are more amenable to bulk isolation through the use of immobilized metal affinity chromatography and may be a better choice as a reporter fusion tag. In addition, a 6xHis is a small tag (6 a.a.) which is unlikely to interfere with protein folding or with protein-protein interactions.

Chapter 4: Biochemical and Proteomic Analysis of COBRA using HisCOB

4.1 Introduction

Previous attempts to perform biochemical and proteomic analysis on COB have been unsuccessful due to the low abundance of COB, as it is not readily detected using proteomic methods (Borner et al., 2003; Nühse et al., 2004). While there has been some mixed success extracting COB-mcYFP for biochemical and proteomic analysis, abundance was still an issue and the partial rescue of the *cob-4* mutant by COB-mcYFP questions the reliability of the findings.

COB-mcYFP was previously found to be absent from the cell wall using live-cell imaging, and COB-mcYFP could not be detected in cell wall protein extracts by immunoblotting. These findings are surprising given that Roudier et al. (2005) previously showed COB to be located predominantly in the primary cell wall. Furthermore, co-immunoprecipitation using anti-GFP beads of cytoplasmic protein extracts showed two populations of COB-mcYFP: a band at 90 kDa that potentially corresponded to full-length protein, and a smaller band at 50 kDa suggesting a cleaved form of the protein (Figure 4.1). Identification of this potential cleavage product has been challenging using COB-mcYFP as the abundance is too low for identification using mass spectrometry.

As discussed in Chapter 3, generation of a 6x-histidine tagged COB fusion construct may be able to both fully complement *cob-4* and alleviate the issues in isolating enough protein for biochemical and proteomic analyses by taking advantage of the interaction between 6xHis and divalent cations to isolate sufficient amounts of COB for proteomic analysis (Block et al., 2009).

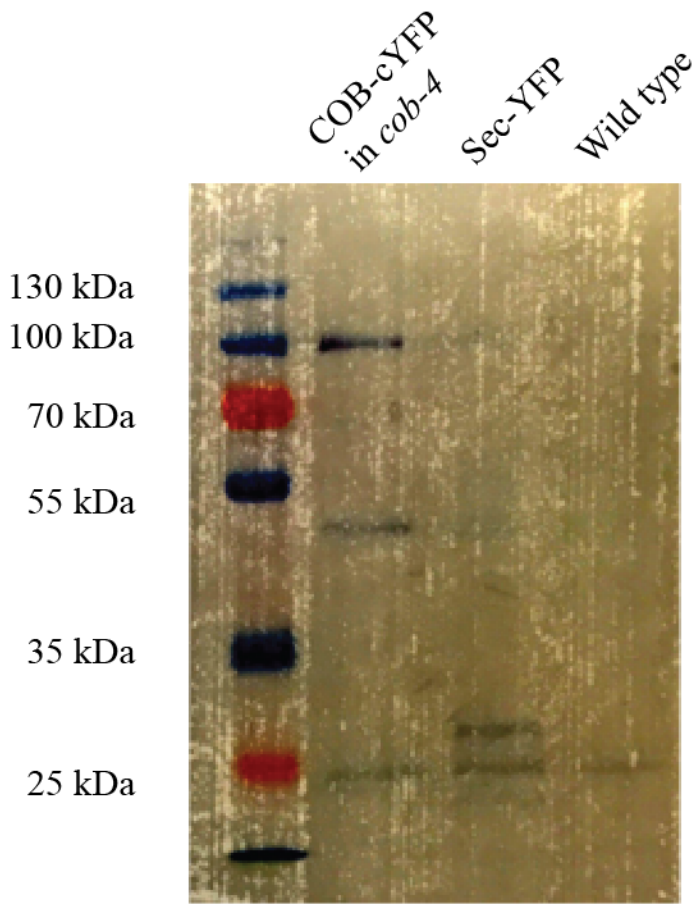

Figure 4.1. Immunoblot of COB-cYFP in *cob-4*

Immunoblot of immunoprecipitated COB-cYFP from total protein extracts using anti-GFP (Sim Ladhar, Wasteneys lab). Two strong bands are visible from COB-cYFP in *cob*-4 – a 100 kDa band representing predicted full-length and a 50 kDa band representing a cleaved peptide. Sec-YFP and wild type immunoprecipitated protein extracts were used as positive and negative controls respectively. The 25 kDa band at the bottom of all 3 lanes represents the light chain of the anti-GFP antibody used in immunoprecipitation.

Successful isolation of a 6xHis-tagged COB should yield protein bands of approximately 48 or 63 kDa depending on the state of glypiation. Though the predicted size is 51 kDa, post-translational removal of the N-terminal signal sequence and the ω-site should yield a 48 kDa protein. While it is unclear how much the addition of the GPI-anchor contributes to the size of COB, a previous study on the rice COBL4 homolog BC1 demonstrated that glypiation

contributed about 15 kDa to the total protein size (L. Liu et al., 2013). Therefore, glypiated COB may have a predicted size of approximately 63 kDa.

The primary objectives of this chapter are to generate 6xHis-tagged COB reporter fusion constructs that will hopefully fully complement the *cob-4* null mutant. If successful, the 6xHis-tagged COB lines will be used to examine the behavior of COB in the cell wall and within the cytoplasm through biochemical and proteomic methods. As previous protein work using COB-mcYFP yielded some results contradictory to those found in Roudier et al. (2005), a 6xHis-tagged COB that is able to fully complement *cob-4* should be able to determine if the findings from using COB-mcYFP were artifacts due to its inability to fully complement *cob-4*.

4.2 Results

4.2.1 COB-His cannot complement *cob-4*

The COB-mcYFP construct, when expressed in the *cob-4* mutant background still yielded a minor phenotype. Its inability to fully restore root length and diameter to wild-type levels could be due to the large size of cYFP. The cYFP was therefore replaced with a much smaller His tag at the same insertion site with identical linker sequences (Figure 4.2). Surprisingly, however, it was not possible to isolate any COB-His lines in a homozygous *cob-4* background despite attempts to segregate 15-20 lines in the T3 and T4 generations. Thus substituting 6xHis at the mcYFP insertion site could not complement *cob-4*.

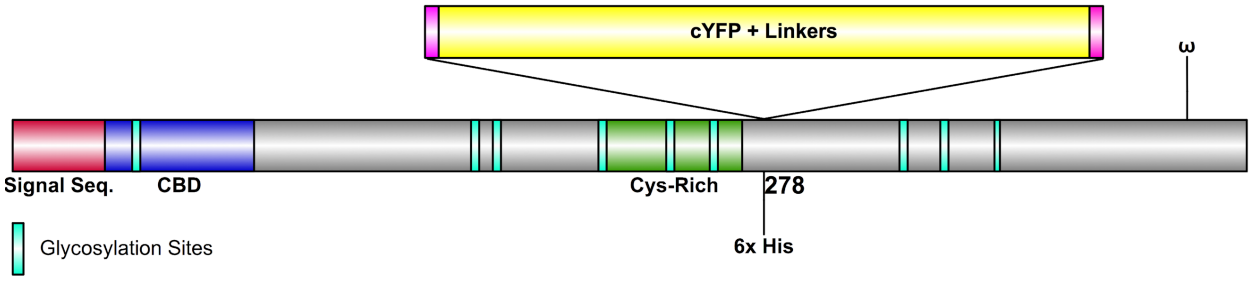

Figure 4.2. Insertion site for COB-cYFP constructs and COB-His

Citrine-YFP and its associate linkers were excised from the COB protein and replaced with a 6xHis tag flanked by linker peptides AGGGA and AAGGG. CBD = cellulose-binding domain and ω = glypiation site.

4.2.2 HisCOB is able to fully complement *cob-4*

After finding that the COB-His construct could not complement *cob-4*, an alternate site for insertion of the 6x-His-tag was sought. Comparison of amino acid homology in the COB family identified a region of low relative homology, just after L183, in COB that may be amenable to insertion of an affinity tag (Figure 4.3). The 6x-his-tag, flanked by linker peptides AGGGA and AAGGG, was inserted after G185 to generate what is hereafter referred to as the HisCOB construct. HisCOB was found to fully complement the *cob-4* null mutant (Figure 4.4A). Measurements of root length and diameter identified no significant difference between HisCOB in *cob-4* and wild type seedlings (Figure 4.4B-C). Analysis of the HisCOB in *cob-4* cellulosic glucose content also showed no difference compared to the wild type, demonstrating that HisCOB can fully complement *cob-4* (Figure 4.4D).

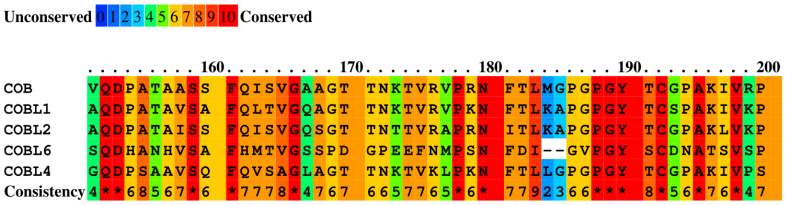

Figure 4.3. Region of low homology in the type I COB gene family

Amino acids M184 and G185 have low homology in COB, suggesting that this region could be amenable to insertion of a fusion tag. Conservation scoring was obtained using PRALINE (Simossis and Heringa, 2005).

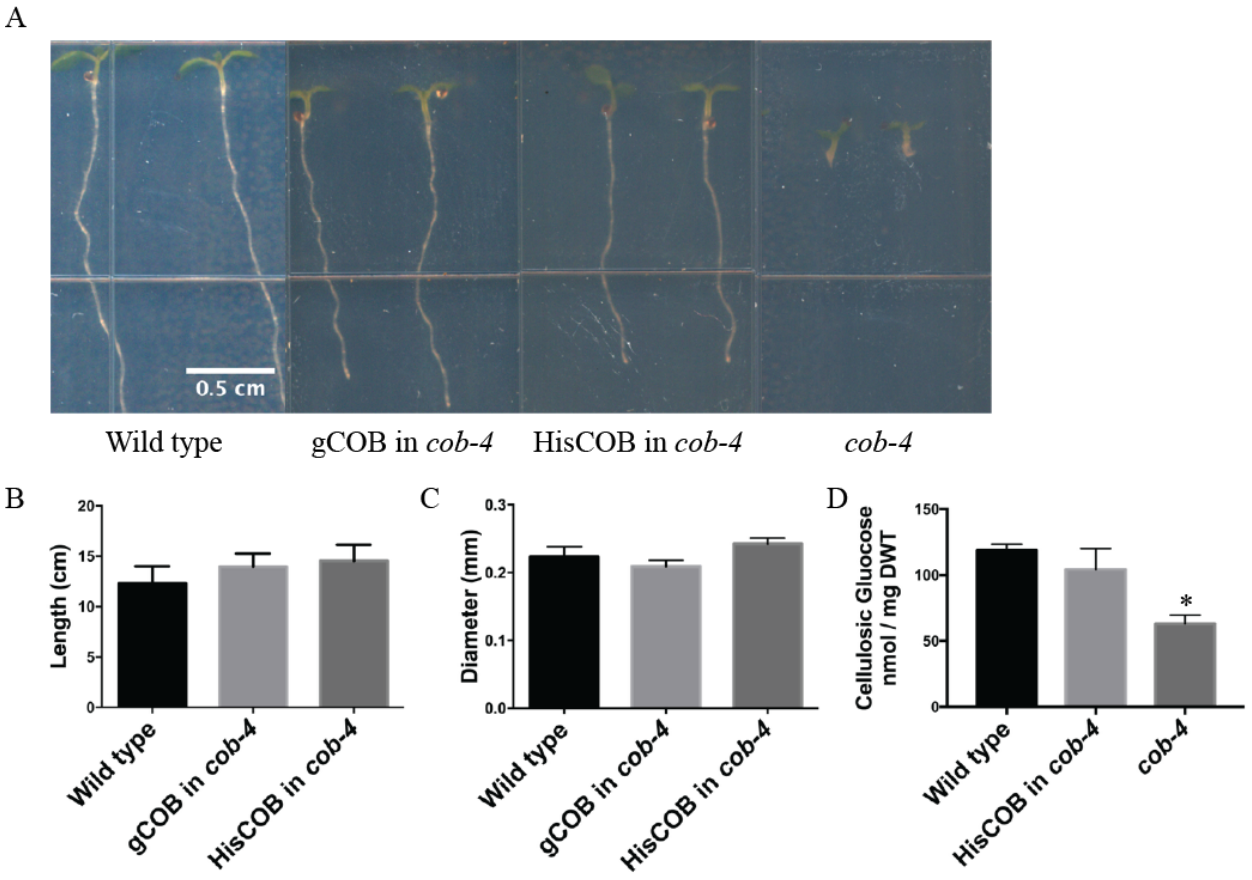

Figure 4.4. HisCOB is able to fully complement *cob-4*

(A) Five-day-old seedlings. gCOB is genomic COB DNA without any tags driven by the native *COB* promoter. HisCOB is able to fully complemented the seedling lethality of *cob-4*, and shows no phenotypic difference to both wild type and gCOB in *cob-4*. Phenotypes were determined from at least three individually transformed lines. (B, C) Root length (B) and diameter (C) measurements of five-day-old seedlings show that HisCOB in *cob-4* is indistinguishable from wild type and gCOB in *cob-4*. Values are mean ± S.E., N > 35. (Tukey's test, $p > 0.05$). (D) Cellulose level is restored to wild-type levels in HisCOB (Tukey's test, * = $p < 0.0001$). Values are mean ± S.E. from more than 3 biological replicates and 2 technical replicates, 1-1.5g of start plant material. DWT = dry weight tissue.

4.2.3 HisCOB is at low abundance and undergoes cleavage in the cell wall

In order to examine if HisCOB was found in the cell wall as indicated by immunogold TEM work (Roudier et al., 2005), cell wall protein extracts were assessed by immunoblotting

using an anti-6xHis antibody. Initial cell wall protein extracts yielded no visible bands, suggesting that HisCOB is absent in the cell wall. To determine if abundance was why HisCOB was unable to be readily detected, the cell wall protein extracts were precipitated and concentrated using trichloroacetic acid (TCA) (Figure 4.5). The $CaCl_2$ and LiCl fractions correspond to proteins that are loosely or tightly bound to the cell wall depending on their interactions with pectin or cellulose respectively (Feiz et al., 2006; Printz et al., 2015).

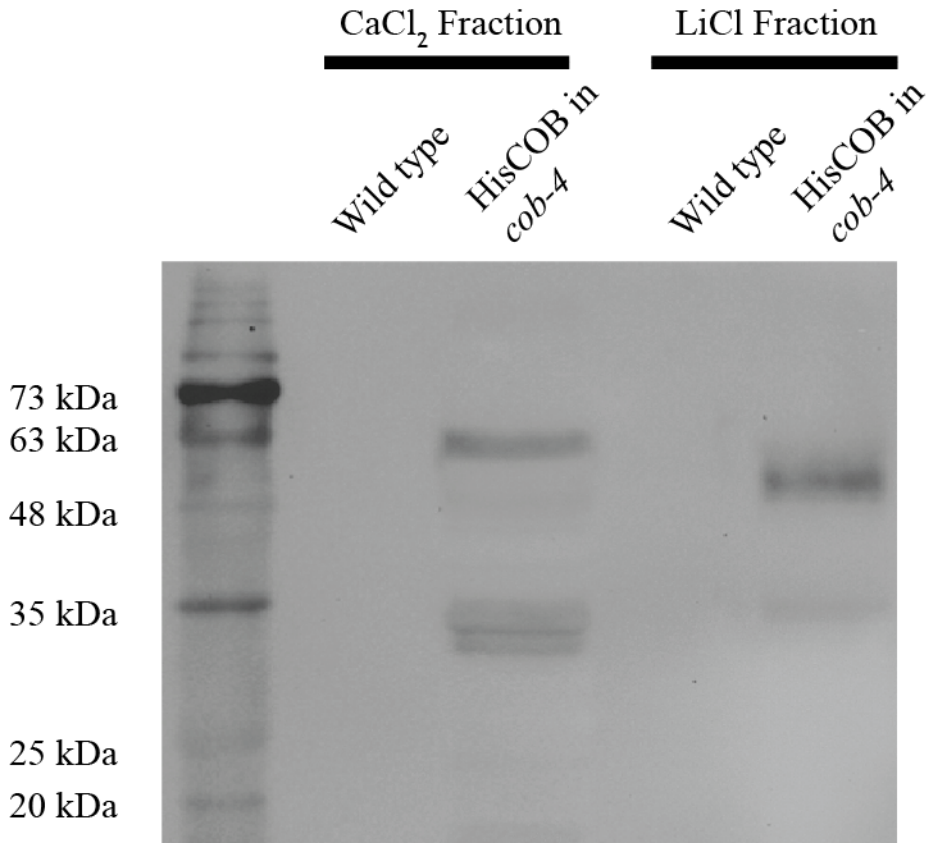

Figure 4.5. Immunoblot of HisCOB cell wall protein extracts

Immunoblot of cell wall protein extracts from wild type and HisCOB in *cob-4* seedlings using anti-His antibody. $CaCl_2$ and LiCl fractions represent pectin-associated proteins and cellulose-associated proteins respectively. Two bands are visible in the $CaCl_2$ fraction of HisCOB in *cob-4* at 63 and 33 kDa, representing full-length HisCOB protein and a smaller polypeptide. Two bands are also visible in the LiCl fraction of HisCOB in *cob-4* at 52 kDa and 33 kDa respectively, possibly representing an un-/de-glypiated HisCOB protein and a smaller polypeptide. Visible bands were present only when the eluate underwent a 20-fold precipitation/concentration step, indicating low cellular abundance.

Immunoblotting of the concentrated samples yielded three distinct bands at approximately 63, 52, and 33 kDa in HisCOB but no bands in wild type, suggesting that HisCOB may exist as three distinct populations in the cell wall (Figure 4.5). The 63 kDa band in the $CaCl_2$ fraction corresponds to the predicted glypiated HisCOB protein (48 kDa post-translationally modified HisCOB + 15 kDa GPI-anchor). The 52 kDa band in the LiCl fraction suggests that HisCOB may undergo a cleavage event in the cell wall. This cleavage event is most likely the removal of the GPI-anchor by a phospholipase as this 52 kDa protein should be tightly bound to the cell wall, and HisCOB has a cellulose binding domain at its N-terminus. In addition, comparison of the band intensities indicate that there is a higher amount of 52 kDa HisCOB compared to the 63 kDa band.

The presence of the 33 kDa band in both the $CaCl_2$ and LiCl fractions indicates that a secondary cleavage event occurs (Figure 4.5). The 33 kDa band is most prominent in the $CaCl_2$ fraction, suggesting that it is cleaved from the 52 kDa band identified in the LiCl fraction and released from the cellulosic tether. Its retention in the $CaCl_2$ fraction indicates that it may interact with the cell wall matrix polysaccharides or with other cell wall proteins.

4.2.4 HisCOB is predominantly a 33 kDa protein in the cytoplasm

Previous immunoblotting of COB-mcYFP cellular extracts showed two bands of COB-mcYFP, one at 90 kDa that potentially corresponded to full-length protein and a smaller band at 50 kDa, consistent with a cleavage event taking place. Cellular protein was therefore extracted from HisCOB/*cob-4* plants and immunoblotted to determine if a similar banding pattern appeared. Whereas immunoblotting of COB-mcYFP required immunoprecipitation from total

cellular extracts using anti-GFP antibody, HisCOB was isolated from total cellular extract using a nickel column.

Visualization of HisCOB on an immunoblot required precipitation of the eluate as there were no detectable HisCOB signal otherwise, consistent with low abundance (Figure 4.6). Interestingly, HisCOB from cellular extracts appeared only as a 33 kDa band, with no detectable band corresponding to full-length protein. This absence of full-length HisCOB could be due to very low cellular abundance or occlusion of the His-tag by the native protein conformation. As this 33 kDa band was also seen in the cell wall protein extracts, this 33 kDa could be endocytosed back into cell from the cell wall or is another secreted form of COB.

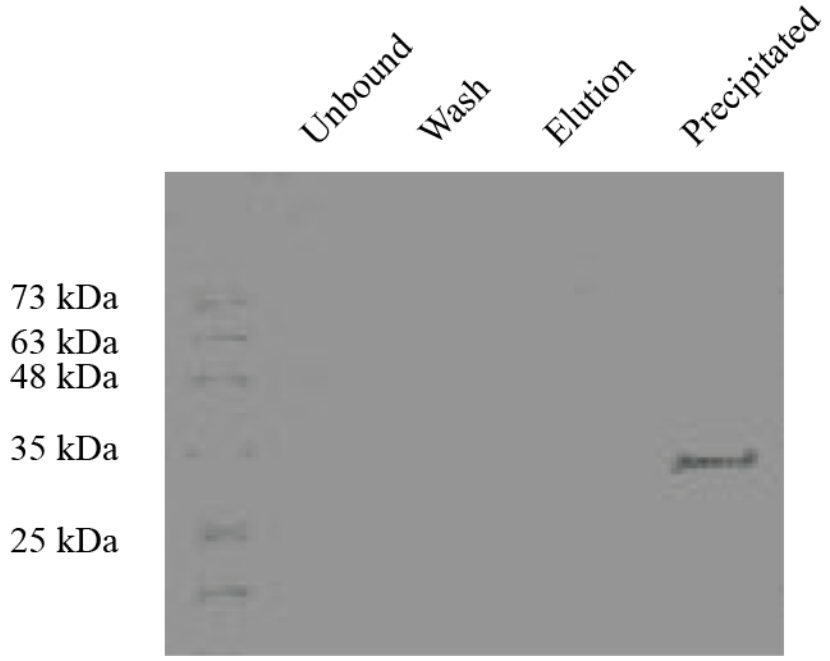

Figure 4.6. Immunoblot of HisCOB purified total cellular protein extracts

Immunoblot of HisCOB purified from total cellular protein extracts using immobilized metal affinity chromatography. Anti-His antibody recognized only a single band at 33 kDa, suggestive of cleavage, and no bands at predicted full-length size (63 or 52 kDa). A visible band was present only when the eluate underwent a 64-fold precipitation/concentration step, indicating low cellular abundance.

In order to determine if the absence of full-length HisCOB from cellular extracts was due to occlusion of the His-tag by the native protein conformation hindering its interaction with the nickel column, purification of cellular extracts was repeated under denaturing conditions (Figure 4.7). Although the 33 kDa band was still the primary band, a 46 kDa band was also visible, which might correspond to un-glypiated full-length protein. This result suggests that the His-tag can be occluded under native conditions. Nevertheless, the absence of full-length (glypiated) protein under native purification conditions indicates that it is in very low abundance.

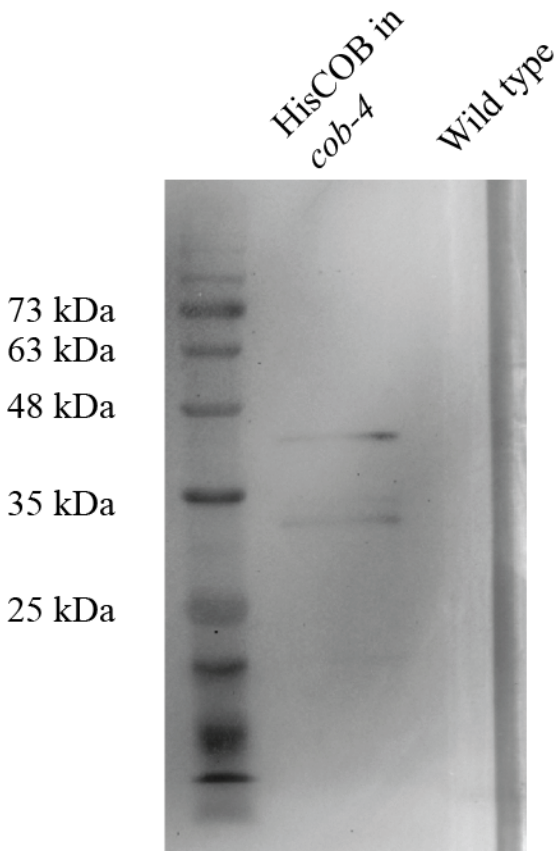

Figure 4.7. Immunoblot of HisCOB purified total cellular protein extracts under denaturing conditions
Immunoblot of HisCOB purified from total cellular protein extracts using immobilized metal affinity chromatography under denaturing conditions. Anti-His antibody recognized a primary band at 33 kDa in addition to a band at 46 kDa suggestive of-unglypiated full-length protein. A visible band was present only when the eluate underwent a 64-fold precipitation/concentration step, indicating low cellular abundance. Purified total cellular protein extracts under denaturing conditions from wild type seedlings were used as a negative control.

4.2.5 Cleavage of HisCOB requires interaction with the cell wall

In order to demonstrate that the 33 kDa band found in the cytoplasm is due to endocytosis from the apoplast, total cellular protein was extracted from HisCOB seedlings after they were plasmolyzed using 0.8 M mannitol for 1 h. Plasmolysis causes the plasma membrane to pull away from the cell wall, which would be expected to inhibit the interaction between COB that is anchored to the plasma membrane and the components of the cell wall. Immunoblotting showed

the disappearance of the 33 kDa band in plasmolyzed seedlings, indicating that the 33 kDa peptide is endocytic and requires the interaction between COB and the cell wall (Figure 4.8). Furthermore, there appeared to be an enrichment of 52 kDa protein in the mannitol-treated seedlings, suggesting that there was accumulation of full-length HisCOB in the cytoplasm when seedlings were plasmolyzed.

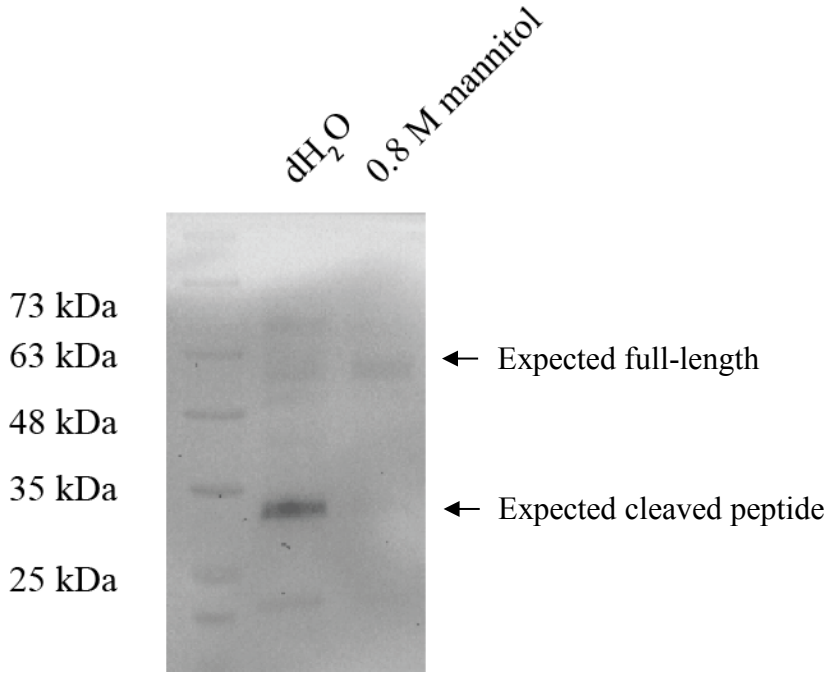

Figure 4.8. Immunoblot of HisCOB from plasmolyzed seedlings

Immunoblot of HisCOB purified from total cellular protein extracts using immobilized metal affinity chromatography from plasmolyzed seedlings. Anti-His antibody recognized only a single band at 33 kDa, in the dH_2O mock treatment. Anti-His antibody did not recognize a 33 kDa band in the 0.8 M mannitol treated seedlings, but there appears to be an enrichment of a band at 63 kDa indicative of full-length HisCOB. A visible band was present only when the eluate underwent a 64-fold precipitation/concentration step, indicating low cellular abundance.

4.2.6 Identification of the 33 kDa HisCOB peptide using LC-MS/MS

Though there is now strong evidence that COB is cleaved as part of its normal function and that the 33 kDa polypeptide is endocytosed, it is still unknown what the function of this

polypeptide is. As there has been evidence that COB can play a regulatory role in transcription, this endocytosed peptide may function as an inducer of signaling cascades (Sorek et al., 2015). Given the difficulties in isolating enough HisCOB for immunoblotting, utilization of HisCOB for co-immunoprecipitation for COB-interactors is likely unfeasible. Alternatively, it may be possible to over-express this 33 kDa peptide in a wild-type background and look for perturbations in growth anisotropy. Furthermore, it may be possible to prevent cleavage from occurring through site-directed mutagenesis if the cleavage site(s) can be identified, which may also cause defects in growth anisotropy.

In order to identify the 33 kDa peptide, it was isolated and partially digested using trypsin before being sequenced using liquid-chromatography mass spectrometry/mass spectrometry (LC-MS/MS). Since partial trypsin digestion can occlude certain peptides via over-digestion, a list of possible identifiable peptides was first generated (Table 4.1).

Sequence	**Start**	**End**
(-)MEFFSR(S)	1	7
(-)MESFFSRSTSIVSK(L)	1	14
(K)LSFLALWIVFLISSSSFTSTEATDALDPEGNITMK(W)	15	49
(K)WDVMSWTPDGYVAVVTMFNFQK(Y)	50	71
(K)WDVMSWTPDGYVAVVTMFNFQKYR(H)	50	73
(K)YRHIQSPGWTLGWK(W)	72	85
(R)HIQSPGWTLGWK(W)	74	85
(R)HIQSPGWYLGWKWAK(K)	74	88
(K)KEVIWSMVGAQTTEQGDCSK(Y)	89	108
(K)EVIWSMVGAQTTEQGDCSK(Y)	90	108
(K)EVIWSMVGAQTTEQGDCSKYK(G)	90	110
(K)YKGNIPHCCK(K)	109	118
(K)GNIPCCK(K)	111	118

Sequence	Start	End
(K)GNIPHCCKK(D)	111	119
(K)KDPTVVDLLPGTPYNQQIANCCK(G)	119	141
(K)DPTVVDLLPGTPYNQQIANCCK(G)	120	141
(K)GGVMNSWVQDPATAASSFQISVGAAGTTNK(T)	142	171
(K)GGVMNSWVQDPATAASSFQISVGAAGTTNKTVR(V)	142	173
(R)VPRNFTLMGPAGGAHHHHHHAAGGGPGPGYTCGPAK(I)	175	211
(R)NFTLMGPAGGAHHHHHHAAGGGPGPGYTCGPAK(I)	178	211
(R)NFTLMGPAGGAHHHHHHAAGGGPGPGYTCGPAKIVRPTK(F)	178	217
(K)FVTTDTR(R)	218	224
(K)FVTTDTRR(T)	218	225
(R)RTTQAMMTWNITCTYSQFLAQR(T)	225	246
(R)TTQAMMTWNITCTYSQFLAQR(T)	226	246
(R)TPTCCVSLSSFYNETIVGCPTCACGCQNNR(T)	247	276
(R)TESGACLDPDTPHLASVVSVLPPLVQCTR(H)	277	305
(R)TESGACLDPDTPHLASVVSVLPPLVQCTRHMCPIR(V)	277	311
(R)VHWHVK(Q)	312	317
(R)VHWHVKQNYK(E)	312	321
(K)QNYKEYWR(V)	318	325
(K)EYWRVK(I)	322	327
(R)VKITITNFNYR(L)	326	336
(K)ITITNFNYR(L)	328	336
(R)LNYTQWNLVAQHPNLDNITQIFSFNYK(S)	337	363
(K)SLTPYAGLNDTAMLWGVK(F)	364	381
(K)FYNDFLSEAGPLGNVQSEILFR(K)	382	403
(K)FYNDFLSEAGPLGNVQSEILFRK(D)	384	404
(R)KDQSTFTFEK(G)	404	413
(K)DQSTFTFEK(G)	405	413
(K)DQSTFTFEKGWAFPR(R)	405	419
(K)GEAFPRR(I)	414	420

Sequence	Start	End
(R)RIYFNGDNCVMPPPDSYPFLPNGGSR(S)	420	445
(R)IYFNGDNCVMPPPDSYPFLPNGGSR(S)	421	445
(R)SQFSFVAAVLLPLLVFFFFSA(-)	446	466

Table 4.1. Possible peptides obtained through partial trypsin digest of HisCOB

List of possible peptides identifiable through LC-MS/MS after partial trypsin digest of HisCOB. Possible peptides were obtained using Protein Prospector from the University of California, San Francisco (prospector.ucsf.edu).

Preliminary sequencing of the 33 kDa peptide band yielded three peptides that mapped to the HisCOB amino acid sequence (Table 4.2). These three peptides represented minimal coverage of the entire protein, so it is thus difficult to draw conclusions on the exact composition of the 33 kDa peptide. Two of the peptides, KDQSTFTFEK and KDPTVVDLLPGTP, however, flank a region of the full-length protein that is approximately 33 kDa in size. There detection is thus of some promise for identifying the cleaved polypeptide found in the immunobots (Figure 4.9).

Sequence	Start	End
LSFLALWIVFLIS	15	27
KDPTVVDLLPGTP	119	131
KDQSTFTFEK	405	413

Table 4.2. List of peptides identified from LC-MS/MS

List of peptides identified from LC-MS/MS after partial trypsin digest of the 33 kDa band isolated from HisCOB total cellular protein extracts.

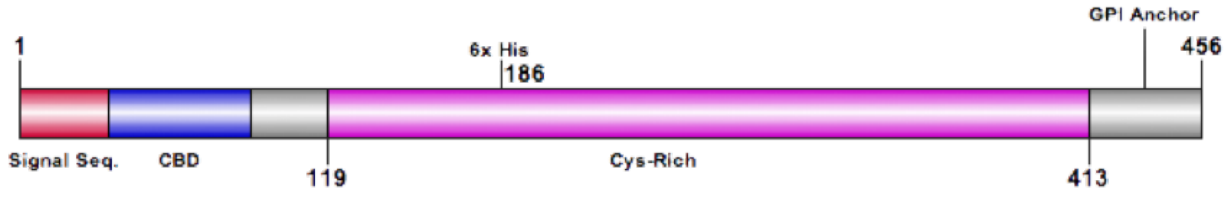

Figure 4.9. Mapping of peptides KDQSTFTFEK and KDPTVVDLLPGTP onto the COBRA protein.

The region (pink) between the two peptides encompasses a 294 amino acid region with a predicted size of 32.6 kDa. This predicted size is similar to that of the excised band that was sequenced. The 6x-His tag is shown to be within the region flanked by the two peptides.

The third peptide identified, LSFLALWIVFLIS, mapped to the very N-terminus of the COB protein, near the signal sequence. Pairing this peptide with either KDQSTFTFEK or KDPTVVDLLPGTP results in a 43 kDa or 13 kDa region respectively, which does not match the 33 kDa peptide that was extracted for sequencing. While this peptide could just be a contaminant, its detection raises the possibility that the other two peptides identified from LC-MS/MS could also be contaminants.

As the low abundance of the 33 kDa band appeared to be the cause of the low coverage, a second sequencing experiment is currently underway using approximately 30 g of plant tissue, a three-fold increase from the preliminary run.

4.3 Discussion

4.3.1 Rescue of the 6xHis-tagged COB reporter fusion constructs

In order to generate a COB reporter fusion construct that could better rescue *cob-4,* a 6xHis tag was inserted at the same site as the cYFP in COB-cYFP, just after S278. While S278 was amenable to insertion of cYFP, it appeared that insertion of a much smaller 6xHis tag at the same location (COB-His) was severely detrimental the function of COB, most likely due to altering protein folding. As the amino acids flanking S278 (PDTPHLASVV**S**PPTKKGTVLP) are highly un-conserved and lack a stretch of hydrophobicity, they are unlikely to play an important role in terms of protein folding. However, insertion of the 6xHis tag with linkers AGGGA and AAGGG does represent an insertion of a hydrophobic-polar-hydrophobic stretch of 16 amino acids, which may be enough to cause a significant change in protein folding, rendering COB-His non-functional.

Interestingly, insertion of the 6xHis tag and links after G185 (HisCOB) in a region relatively high conservation was able to fully complement the *cob-4* null mutant. While the amino acids flanking G185 (VRVPRNFTLM**G**PGPGYTCGPA) are relatively conserved and there is a fairly hydrophobic region immediately downstream of the insertion site, this region was clearly amenable to insertion of the 6xHis tag and linkers. Interestingly, this insertion site is also in close proximity to the *cob-1* point mutation G167A.

4.3.2 Cleavage events of COB

The 63 kDa band identified in the $CaCl_2$ fraction from cell wall protein extracts that matches the predicted size of glypiated HisCOB. The presence of two smaller bands indicated that COB undergoes at least two cleavage events in the cell wall. Based on the LiCl fraction of the cell wall extractions, the first cleavage event appears to be dependent on COB interacting strongly with the cellulose microfibrils, presumably through the cellulose-binding domain, which then causes release of COB from its GPI-anchor leaving the majority (52 kDa) of the protein within the cell wall. It is unlikely that any cleavage events are able to take place at the N-terminal region of COB, as it should be buried within the cellulose microfibrils leaving only the C-terminal region vulnerable to cleavage events. It is likely that this release of COB from its GPI-anchor is caused by a phospholipase, presumably phospholipase D as it was previously shown to de-glypiate the rice COB homolog BC1 in vitro (L. Liu et al., 2013).

More interesting, however, is evidence of a second cleavage event that results in a 33 kDa peptide. While this peptide is present in both $CaCl_2$ and LiCl fractions, its higher abundance in the $CaCl_2$ fraction suggests that the cleavage event causes release of a portion of COB from being bound to the cell wall. In order for the peptide to shift from the LiCl to the $CaCl_2$ fraction, this second cleavage event would need to take place downstream of the cellulose-binding

domain. In addition, the fact that the peptide remains within the $CaCl_2$ fraction after the extraction steps suggests that the peptide is able to interact with other cell wall proteins. Though this 33 kDa peptide presumably lacks both the cellulose-binding domain and GPI-anchor, it may be able to interact with other proteins through its cysteine-rich domain (DeBruine et al., 2017; Schlessinger, 2002; Smulski et al., 2013).

In contrast to the wall extracts, cytoplasmic extracts predominantly contained the 33 kDa HisCOB polypeptide, with full-length protein barely detected. The multiple bands found in the cell wall protein extracts supports a model whereby cleavage of full-length COB takes place in the apoplast, followed by endocytosis of the 33 kDa polypeptide. This model is further supported by the loss of the 33 kDa polypeptide after inhibition of COB secretion via plasmolysis. This finding also argues against this 33 kDa polypeptide being an alternate splice product of *COB*.

As COB has been previously implicated to have a role in transcriptional regulation, endocytosis of a cleaved portion of COB could provide a mechanistic link between COB's function in the cell wall and its proposed role in transcriptional regulation (Sorek et al., 2015). Once within the cell, the peptide may function to trigger signal transduction cascades which ultimately results in modification of the plant primary cell wall. Furthermore, a previous preliminary pull-down experiment using COB-dcYFP found a subunit of the mediator complex, MED32, as a potential direct interactor with COB (Fujita et al., unpublished). However, as the pull-down was done using COB-dcYFP there is some doubt on the validity of this interaction.

4.3.3 A new model for COBRA trafficking

The presence of cleavage in the HisCOB protein extracts gives credence to the immunoblots previous performed on COB-mcYFP, which also showed the presence of a smaller, cleaved peptide from cytoplasmic protein extracts. In contrast, COB-mcYFP had the cleaved

peptide as a minor product and the major product was putative full-length protein, unlike the HisCOB immunoblots. As HisCOB was able to fully complement *cob-4* and COB-mcYFP was not, the accumulation of full-length COB-mcYFP may be an artifact as a result of partial functionality.

In contrast to HisCOB, COB-mcYFP was not detected in the cell wall. The overaccumulation of full-length COB-mcYFP protein in the cytoplasm could give a mechanistic explanation as to why COB-mcYFP can only partially rescue. As full-length HisCOB was rarely detected in the cytoplasm, it is likely that it is readily secreted out to the apoplast where it is primarily localized. However, as full-length COB-mcYFP is readily detected in the cytoplasm, it is likely that the addition of mcYFP hinders its secretion resulting in accumulation within the Golgi and/or secretory vesicles. While COB-mcYFP is still able to reach the apoplast and interact with cellulose, as evidenced the presence of cleaved COB-mcYFP in the cytoplasmic protein extracts, it is present in such low quantities that it cannot be detected in the cell wall protein extracts. As such, the partial rescue of COB-mcYFP is likely due to insufficient COB-mcYFP reaching the apoplast and interacting with cellulose. This retardation of COB-mcYFP secretion would also help explain why COB-mcYFP is not readily detected in the cell wall or at the plasma membrane using live-cell imaging and is instead primarily found in the Golgi or small puncta. Furthermore, this suggests that amount of the cleaved COB is important for the function of COB, again suggesting the COB may have an important role in signaling.

In summary, the evidence from this study suggests that native COB is rapidly secreted to the apoplast where it is primarily found bound to the plasma membrane via its GPI-anchor. Once out in the apoplast, COB can then bind directly to the cellulose microfibrils via its cellulose-binding domain or potentially interact with other cell wall proteins or loosely interact with non-

cellulosic cell wall polysaccharides. Once tightly bound to cellulose, COB is released from its GPI-anchor and is no longer bound to the plasma membrane. Once free from the plasma membrane and bound to cellulose, a secondary cleavage event occurs downstream of the cellulose-binding domain releasing a portion of the COB protein from the cell wall. This cleaved 33 kDa peptide could possibly interact with either full-length COB or other cell wall proteins before being endocytosed. Though it is currently unknown what happens to this peptide after endocytosis, it might interact with intracellular receptors to trigger signal transduction cascade(s) ultimately resulting in modification of the primary cell wall (Figure 4.10). When COB is conjugated with the mcYFP, exocytosis is retarded resulting in an accumulation of full-length COB-mcYFP in the Golgi and secretory vesicles and a decrease in apoplastic COB-mcYFP.

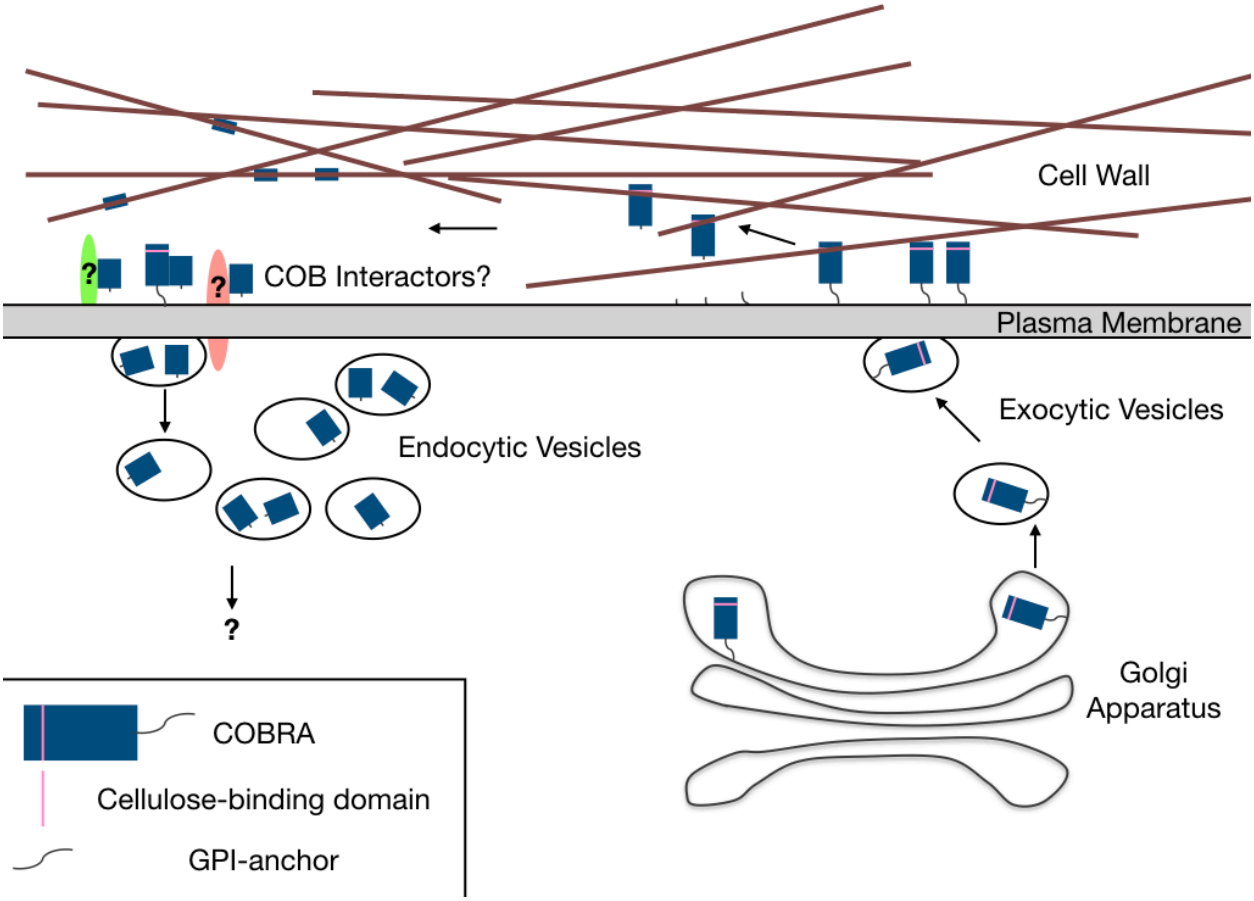

Figure 4.10. Proposed model of COBRA Trafficking

Full-length COB is rapidly secreted to apoplast where it is bound to the plasma membrane. COB is then able to bind to the cellulose microfibrils (brown) via its cellulose binding domain, which triggers cleavage of a portion of the GPI-anchor release COB from the plasma membrane. Once released from the plasma membrane, COB can then undergo a second cleavage event downstream of the cellulose-binding domain freeing the majority of the protein from the cell wall. This free peptide may then interact with other cell wall proteins (green and pink) before ultimately being endocytosed. The final destination of this peptide is currently unknown.

4.3.4 Proposed function of COBRA

As previously mentioned, there is evidence that COB may play an important role in primary cell wall biosynthesis by as a regulatory protein (Sorek et al., 2015). While it was previously hypothesized that COB is an important structural component of the primary cell wall, its low abundance in the cell wall and the new model of COB trafficking makes that hypothesis

unlikely (Roudier et al., 2005). Instead, it is likely that COB acts a regulator of primary cell wall biosynthesis, perhaps by monitoring cellulose quality or crystallinity, by modulating transcription. While there has been no evidence of such a regulator in the literature, there does need to be a mechanism for the plant cell to monitor the production of cellulose. Given the importance of COB in cellulose biosynthesis and the evidence presented here it is possible that COB is responsible for monitoring cellulose biosynthesis, and that COB knock-outs, such as *cob-4*, are unable to monitor cellulose production resulting in a loss of growth anisotropy and ultimately death.

Chapter 5: Identification of Important COBRA Protein Domains

5.1 Introduction

While several protein domains have been identified in COBRA based on homology, there has been little experimental evidence on the exact functions of each of these domains. For example, while the cellulose-binding domain was one of the first regions identified, it was not until recently that its importance has been demonstrated as seen in the rice COBL4 homolog BC1 (L. Liu et al., 2013; Roudier et al., 2002). In addition, there may be other important protein domains with COB that are still unidentified due to the limitations and difficulties of working with this protein.

The sucrose-dependent phenotypes of certain mutants such as the point mutants *cob-1* and *hulk-1* also suggest the importance of specific amino acids in the COB protein, though their importance is still poorly understood (Seifert, unpublished; Schindelman et al., 2001). However, the commonality of sucrose being an inducer of these phenotypes suggest that the mutated amino acids may share a similar function. As the HisCOB insertion site is in close proximity to both the *cob-1* and *hulk-1* point mutations, perhaps it also has a sucrose-dependent phenotype (Figure 5.2).

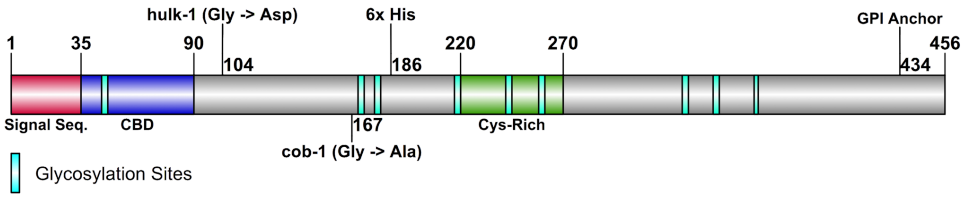

Figure 5.1. HisCOB insertion site and *cob-1* and *hulk-1* point mutations are in close proximity

One important domain of interest that has not been well explored is the highly conserved cysteine-rich domain. Attempts to generate truncations in the cysteine-rich domain have resulted in unviable plants, suggesting an important functional or structural role. While the cysteine-rich

domain has been shown to be important for protein-protein interactions in animal cells, this area is relatively unexplored in plant cells (DeBruine et al., 2017; Schlessinger, 2002; Smulski et al., 2013). As the findings from Chapter 4 suggest that the cleaved COB peptide lacks the cellulose-binding domain but is still retained in the cell wall, COB may be able to interact with other cell wall proteins or even with itself through its cysteine-rich domain.

In addition, it has yet to be determined if COB's function is dependent on its interaction with cellulose. While COB does have a putative cellulose-binding domain (CBD), it has not been shown if COB can bind directly to cellulose. A rice homolog of *COB*, *BC1* has been shown to require two specific aromatic amino acids, Y46 and W72, in the CBD in order to properly bind to cellulose (L. Liu et al., 2013). Replacement of either of these residues with the aliphatic amino acid alanine resulted in a severe reduction in the ability of $bc1^{Y46A}$ and $bc1^{W72A}$ to bind to cellulose and a significant reduction in cellulosic glucose (L. Liu et al., 2013). As there is a high degree of homology in the CBMs, it is possible to replicate the BC1 Y46A and W72A amino acid substitutions in COB in order to examine their importance in COB's function. For example, if COB-mcYFP was unable to interact with cellulose there may be build-up of COB-mcYFP at the plasma membrane and/or apoplast which could be easily visualized using live-cell imaging.

The primary goals of this chapter were to examine if HisCOB also had a sucrose-dependent phenotype and to examine if COB could function as a homodimer. A secondary goal was to determine if COB's function is dependent on its ability to bind to cellulose.

5.2 Results

5.2.1 HisCOB exhibits a sucrose-dependent radial swelling phenotype

While HisCOB is able to fully complement *cob-4* when grown on media lacking sucrose (Chapter 4, Fig. 4.4), when grown on media supplemented with 4.5% sucrose HisCOB exhibits a

radial swelling phenotype reminiscent to that of the *cob-1* point mutant, but less severe (Figure 5.2A) (Schindelman et al., 2001). Comparison with wild-type and *cob-1* seedlings grown on media supplemented with 4.5% sucrose showed a reduction in HisCOB root length and an increase in root diameter, but not to the same extent as *cob-1* (Figure 5.2B-C).

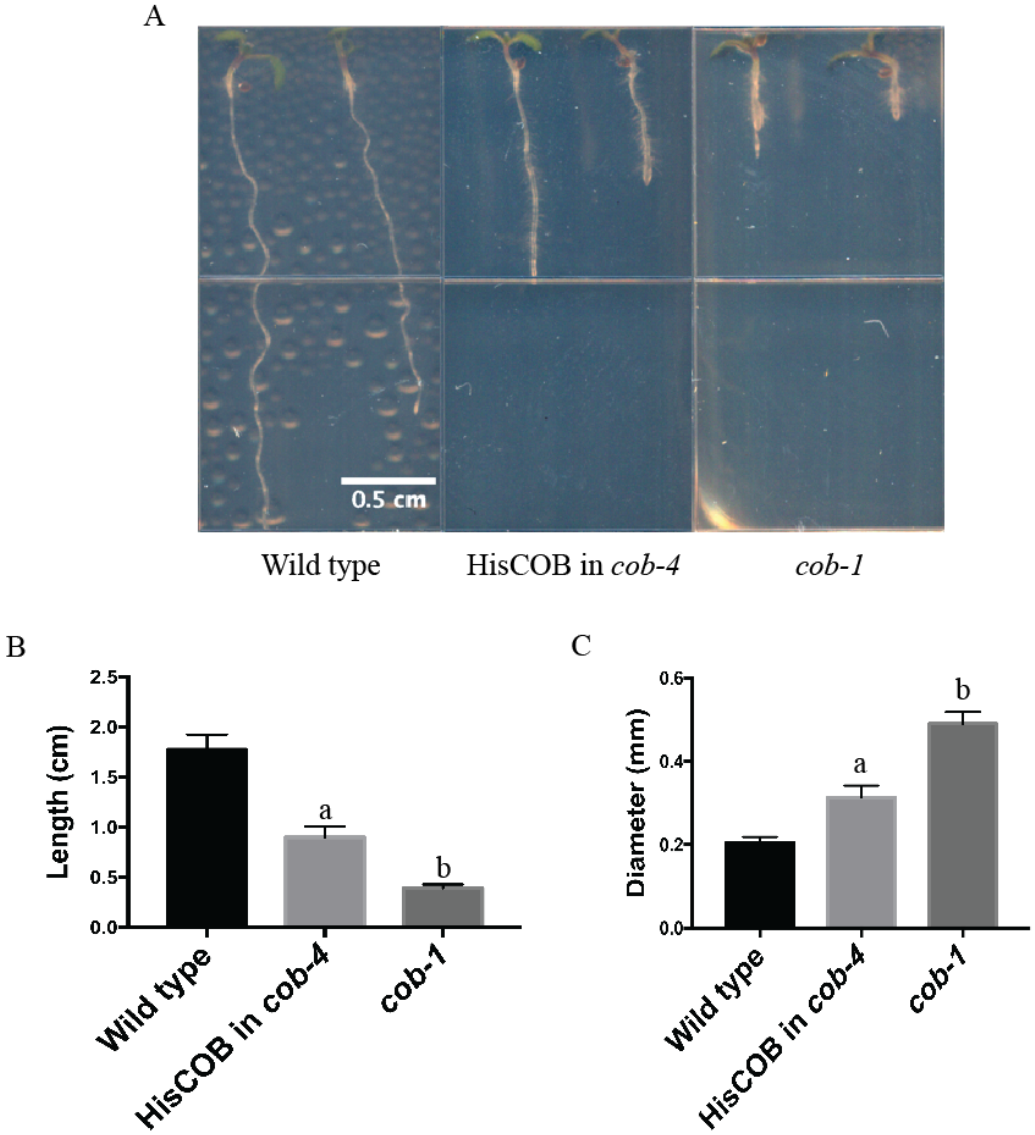

Figure 5.2. HisCOB has a sucrose-dependent phenotype

(A) Five-day-old seedlings grown on media supplemented with 4.5% sucrose. Wild type growth anisotropy is not perturbed by the addition of sucrose, while both HisCOB and *cob-1* show a reduction in root length and radial swelling. (B, C) Root length (B) and diameter (C) measurements of five-day-old seedlings grown on media supplemented with 4.5% sucrose shows significant reductions in root length and increase in root diameter, demonstrating a loss of growth anisotropy. Values are mean ± S.E., N > 35. Letters denote statistical differences between groups (Tukey's test, $p < 0.05$).

5.2.2 HisCOB x *cob-1* transheterozygotes have an intermediate phenotype

Given that HisCOB and *cob-1* both have a radial swelling phenotypes on media supplemented with sucrose and are in close proximity with one another, this region may be important for the function of COB. In order to explore this, the HisCOB in *cob-4* and *cob-1* were crossed with one another and the F1 transheterozygotes examined. These F1s, which contain a single copy of HisCOB in a *cob-1*/*cob-4* mutant background, have an intermediate phenotype between that of the two parental lines (Figure 5.3A). While root length was significantly increased compared to *cob-1*, it was still not restored to *HisCOB*/*cob-4* levels. Nevertheless, this still suggests the ability for HisCOB to partially complement *cob-1* (Figure 5.3B). However, the F1 transheterozygotes still had severe radial swelling similar to that of *cob-1*, and there was no complementation of this phenotype by HisCOB (Figure 5.4C).

These findings suggest that there may be interaction between HisCOB and the *cob-1* protein, though it is unclear if this interaction is direct, such as through dimerization, or indirect by interacting with other proteins. In addition, since the *cob-1* and *hulk-1* point mutations, and the HisCOB transgene are in close relative proximity to the putative cleavage site identified in Chapter 4, the conditional radial swelling phenotypes may be caused by altered cleavage during sucrose-induced rapid elongation, preventing COB from functioning properly as a monitor of cellulose (Figure 5.4)

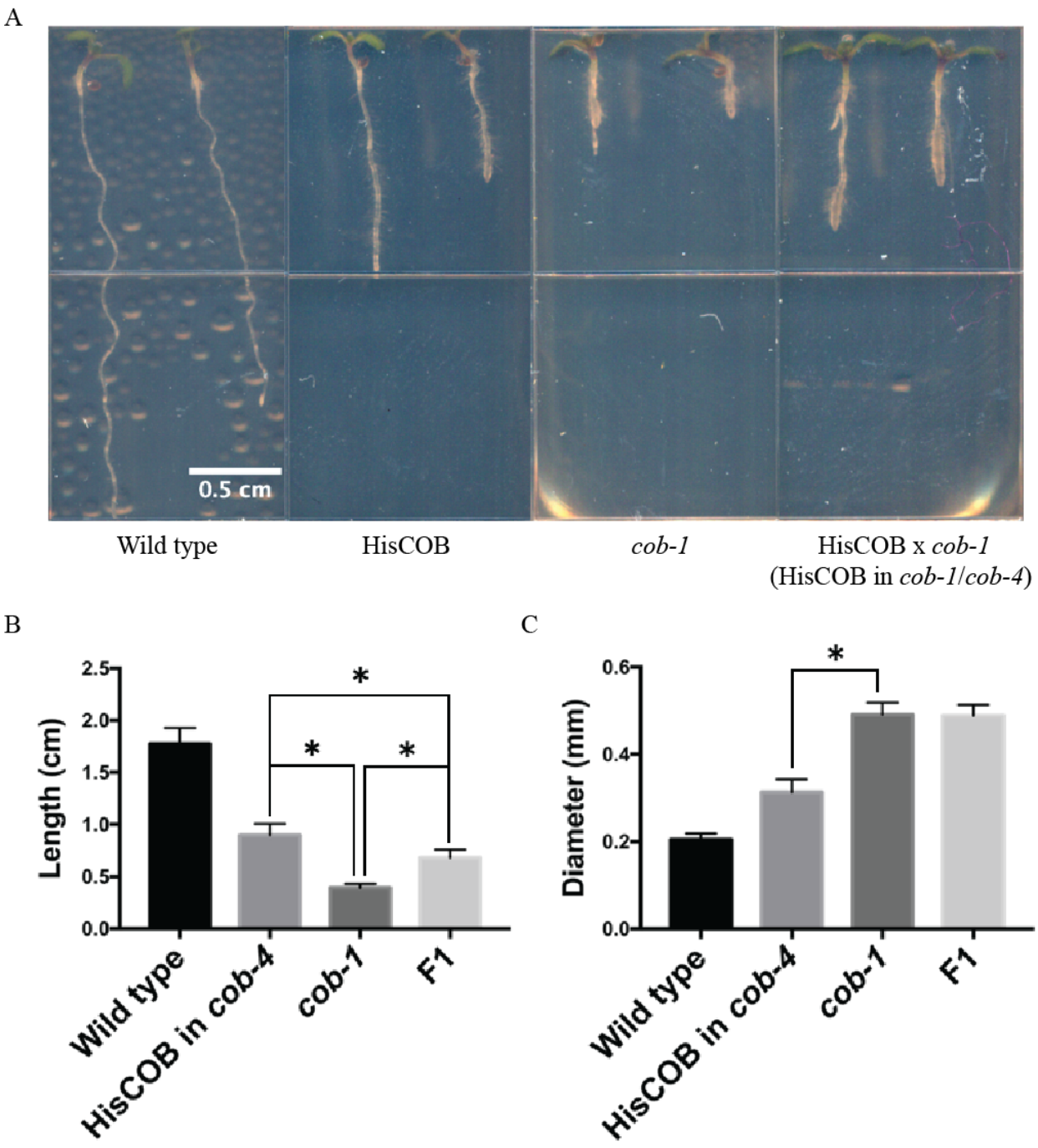

Figure 5.3. HisCOB can partially complement *cob-1*

(A) Five-day-old seedlings germinated on medium supplemented with 4.5% sucrose. HisCOB x *cob-1* transheterozygotes have an intermediate phenotype compared to HisCOB or *cob-1* alone. (B, C) Root length (B) and diameter (C) analysis of five-day-old seedlings indicate that the transheterozygotes have increased root length but no changes in root diameter. Values are mean ± S.E., N > 35. Relevant statistics are shown, asterisks denote statistical differences between groups (Tukey's test, $p < 0.05$).

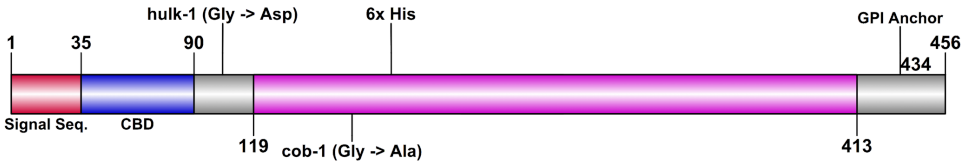

Figure 5.4. HisCOB, *cob-1*, and *hulk-1* are in close proximity to the predicted peptide cleavage site
Pink denotes the 33 kDa peptide region identified in chapter 4 through LC-MS/MS

5.2.3 Cleavage of HisCOB is unaffected by sucrose

As HisCOB exhibits a radial swelling and loss of growth anisotropy phenotype when grown on media containing 4.5% sucrose, it was hypothesized that the addition of the His-tag may interfere with cleavage when rapid elongation is induced by the addition of sucrose. Preliminary findings from the total protein extracts of HisCOB seedlings grown on media containing 4.5% sucrose, however, showed no apparent changes in the amount of cleavage (Figure 5.5). This finding suggests that insertion of the 6x-His tag in COB does not prevent sucrose-induced cleavage. While it remains possible that the HisCOB protein undergoes increased cleavage in the presence of 4.5% sucrose, the requirement to affinity purify HisCOB renders quantification difficult.

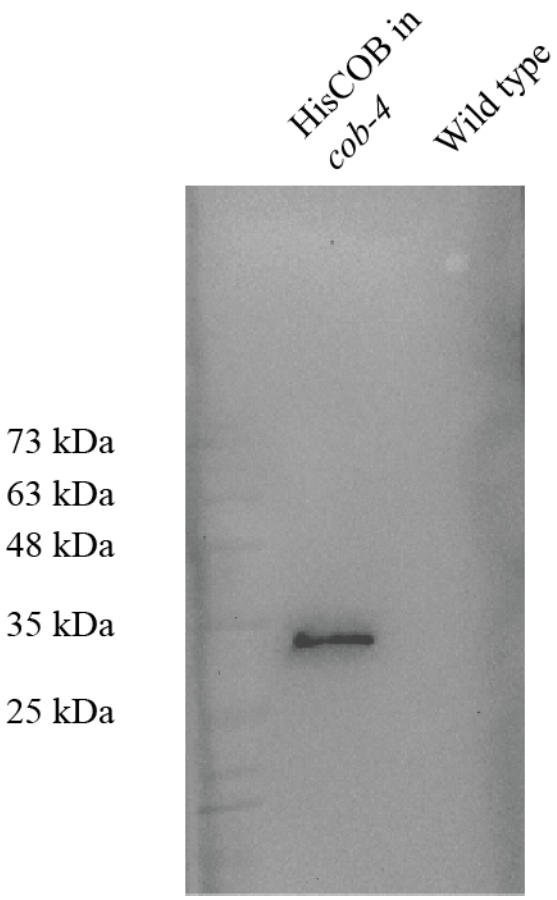

Figure 5.5. Immunoblot of sucrose-induced radially-swollen-HisCOB purified from total cellular protein extracts

Immunoblot of HisCOB protein purified from total cellular protein extracts using immobilized metal affinity chromatography from HisCOB in *cob-4* grown on medium supplemented with sucrose. Anti-His antibody still only recognized a band at 33 kDa band suggesting that the conditional radial swelling phenotype is unrelated to cleavage. A visible band was present only when the eluate underwent a 20-fold precipitation/concentration step, indicating low cellular abundance. Total cellular protein extracts under denaturing conditions from wild type seedlings grown on medium supplemented with sucrose were used as a negative control.

5.2.4 COB-mcYFP in combination with wild type COB exhibits reduced root growth

If COB function depends on homodimerization, a mismatch between a tagged and untagged version of the protein could interfere with its normal function generating a mutant phenotype. To test this possibility, the COB-mcYFP, HisCOB and gCOB, an un-tagged version of COB genomic DNA, were transformed into wild-type seedlings, rather than the *cob-4* null

allele. Expression of HisCOB or gCOB in wild-type backgrounds yielded no radial swelling phenotypes, suggesting that having 4 similar-sized copies of COB does not negatively affect plant growth (Fig. 5.6A). Quantification of root length (Fig. 5.6B) and diameter (Fig. 5.6C) for HisCOB or gCOB in wild-type seedlings confirmed that there were no obvious changes in growth anisotropy.

When COB-mcYFP was expressed in the wild-type background, there was significant reductions in root length, although root diameter was unchanged (Fig. 5.6A-C). While root length is reduced, diameter is unchanged suggesting a minor perturbation of growth anisotropy. This finding suggests that COB-mcYFP interferes with the function of wild-type COB. This could be due to competition between wild type and recombinant COB or to COB-mcYFP negatively affecting the function of the endogenous COB.

Attempts to segregate COB-mcYFP and HisCOB in wild-type lines from the *cob-4* heterozygous backgrounds were unsuccessful, suggesting incompatibility between the tagged-COB and endogenous COB during segregation. However, it is interesting that direct transformation of HisCOB into a wild-type background caused no obvious phenotype.

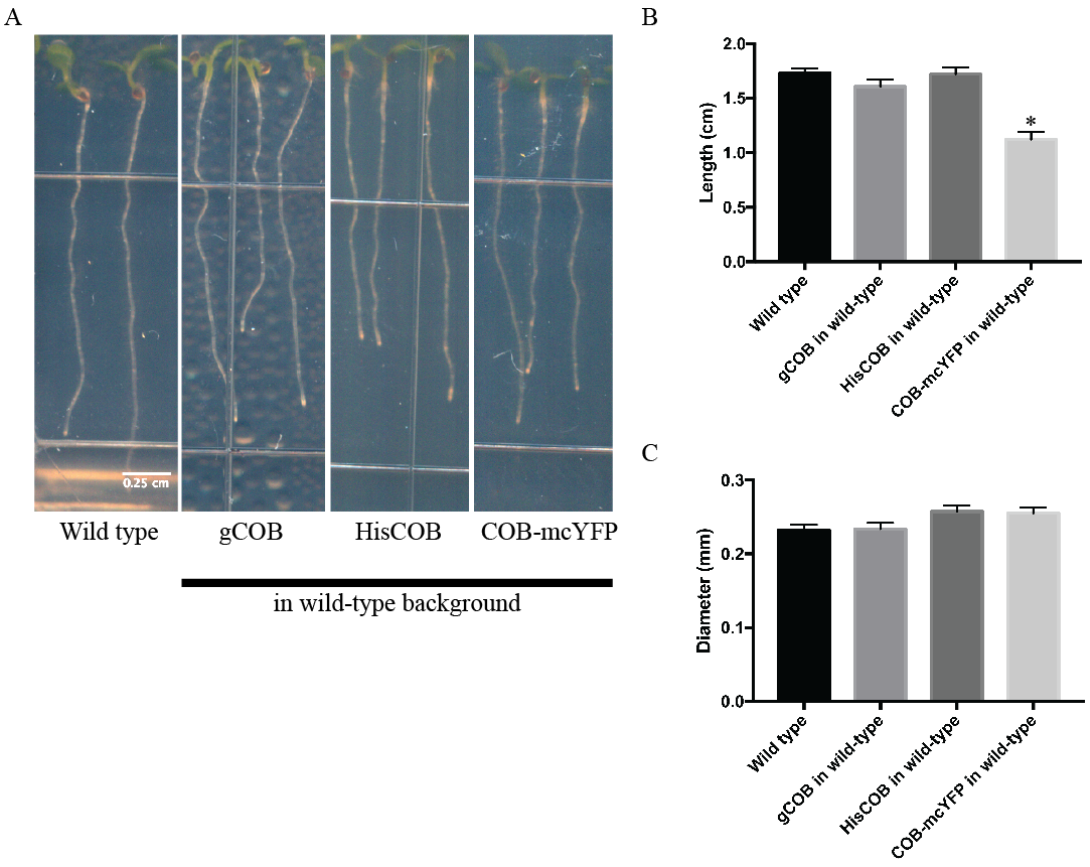

Figure 5.6. COB-mcYFP in wild-type background has reduced root length

(A) Five-day-seedlings. COB-mcYFP in the wild type background has reduced root length while gCOB and HisCOB do not. Phenotypes were determined from at least three individually transformed lines. (B, C) Analysis of the root length (B) and diameter (C) of five-day-old seedlings indicated no changes in root diameter but a reduction in COB-mcYFP in wild-type root length. Values are mean ± S.E., N > 35. Asterisks denote statistical differences between groups (Tukey's test, $p < 0.05$).

5.2.5 Amino acids Y60 and W86 are important to COB function

In order to examine the interaction between COB and cellulose, site-directed mutagenesis was performed on COB-cYFP to mutate specific residues in the cellulose-binding domain. Previous work by Liu et al. (2013) demonstrated the importance of amino acids Y46 and W72 in cellulose binding in the rice COB homolog BC1, which map to Y60 and W86 respectively in COB (Figure 5.7). While the Y60A-COB-cYFP and W86-COB-cYFP constructs were able to

complement the seedling lethality of *cob-4*, the plants are severely dwarf with radial swollen roots (Figure 5.8A). Furthermore, leaf production and rosette growth were delayed or hindered in these seedlings (Figure 5.8A)

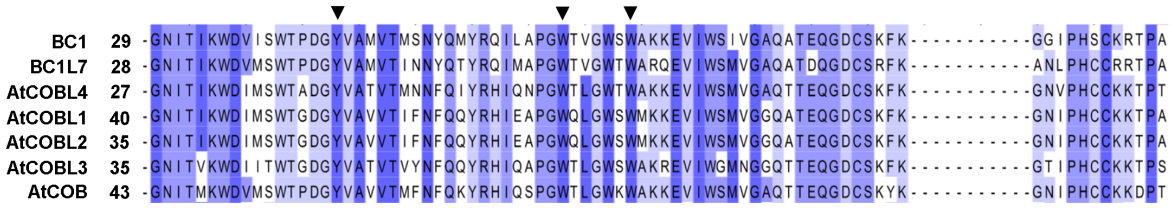

Figure 5.7. Alignment of the BC1 cellulose binding domain with selected homologs

Arrows denote the aromatic residues important for function of the cellulose-binding domain. Amino acids Y40 and W72 in BC1, which correspond to Y60 and W86 in AtCOB, were found to be most necessary for cellulose binding. Adapted from "Brittle Culm1, a COBRA-Like Protein, Functions in Cellulose Assembly through Binding Cellulose Microfibrils," by L. Liu et al., 2013, *PLOS Genetics, 9*(8), Supplemental S2. Copyright 2013 by L. Liu et al.

Unlike other *cob* mutants, Y60A-COB-cYFP and W86-COB-cYFP exhibit severe developmental defects past the seedling stage. These lines were unable to survive on soil and had to be grown in magenta boxes containing Hoagland's media. Y60A-COB-cYFP and W86-COB-cYFP seedlings had a loss of apical dominance causing early branching of the inflorescence stem, in addition to defects in silique development (Figure 5.8B). These lines were ultimately sterile and could not be further propagated, suggesting that COB functions by interacting with cellulose via Y60 and W86. Furthermore, the severe phenotypes seen past the seedling stage suggest that COB's function is important throughout plant development, despite its high expression in cells undergoing rapid elongation.

A B

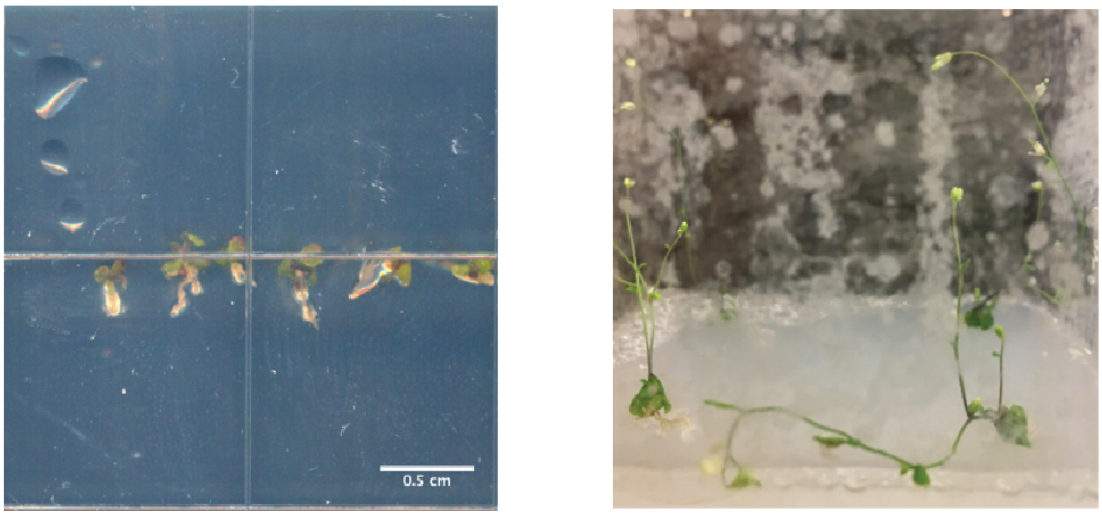

Figure 5.8. COBRA cellulose-binding domain mutants have a severe phenotype

(A) Ten-day-old Y60A-COB-mcYFP seedlings. Seedlings have severely stunted growth and loss of growth anisotropy. Seedlings also appear to be developmentally delayed as evidenced by their lack of leaf production and rosette growth. (B) Y60A-COB-mcYFP seedlings 25 days after germination. Seedlings cannot survive on soil and must be grown within magenta boxes on media. Seedlings have reduced rosette size in addition to a loss of apical dominance as evidenced by early branching of the stem. There is also pre-mature silique production, and the siliques are ultimately sterile. W86A-COB-mcYFP (not shown) has identical phenotypes to Y60A-COB-mcYFP.

5.2.6 Y60A-COB-mcYFP in wild type has a dominant negative phenotype

In order to further explore to possibility that COB may be able to form homodimers, the mutated cellulose binding domain Y60A-COB-mcYFP construct was transformed into the wild-type background. Though these seedlings are still in the early stages of the transformation process and still need to be segregated, the T1 seedlings exhibit severe radial swelling in in the lateral roots (Figure 5.9). This is unlike other *cob* mutant phenotypes, in which radial swelling is generally restricted to the primary root and the lateral roots are unaffected.

Figure 5.9. T1 Y60A-COB-mcYFP in wild type

The fact that a more severe phenotype is seen in Y60A-COB-mcYFP in wild type compared to COB-mcYFP in wild type can be attributed to Y60A-COB-mcYFP's predicted inability to interact with cellulose. This demonstrates that Y60A-COB-mcYFP interferes with the endogenous COB function more severely than the unmutated COB-mcYFP.

5.3 Discussion

5.3.1 COBRA and its relation to sucrose

As *cob-1*, *hulk-1*, and HisCOB all exhibit conditional phenotypes when grown on media supplemented with sucrose there appears to be some important relationship between the function of COB and sucrose. However, it is unknown if these phenotypes are triggered by the rapid root elongation induced by sucrose, or through other sucrose-related mechanisms. As there appears to be no changes to the ability of HisCOB to undergo cleavage when grown on 4.5% sucrose media, it is unlikely that HisCOB's sucrose-dependent phenotype is cleavage related. However, as there are currently no tagged- versions of *cob-1* or *hulk-1*, it is not known if the conditional phenotypes in these mutants are related to cleavage.

It remains why these COB mutants can cause such drastic loss of anisotropic growth when grown on 4.5% sucrose medium. While it has been previously shown that *cob-1* on 4.5% has a reduction in crystalline cellulose and disorganization of cellulose microfibrils, the exact cause is unknown (Schindelman et al., 2001). It was previously hypothesized that the G167A substitution in *cob-1* interfered with its role as a structural protein, but the findings shown in Chapter 4 suggests that COB plays a non-structural role in the cell wall. The possibility that the reduction in cellulose crystallinity and microfibril disorganization is caused by transcriptional changes remains to be determined.

5.3.2 COB's cysteine-rich domain may be important for protein-protein interactions

As discussed previously, cysteine-rich domains have been shown to be important for protein-protein interactions in animal systems but have not been well characterized in plants. A possible explanation for the partial rescue of COB-mcYFP in *cob-4* could be masking of the cysteine-rich domain due to the close proximity of the insertion site and mcYFP's relative bulkiness. Furthermore, the reduction in root length seen in COB-mcYFP in wild type and not HisCOB or gCOB suggests possible interference between recombinant and endogenous COB.

Furthermore, the severe dominant-negative phenotype seen in the Y60A-COB-mcYFP in wild-type line suggests that there may direct interactions between COB proteins, such as formation of a COB heterodimer composed of a functional wild-type COB and a non-functional Y60A-COB-mcYFP. However, there is still little evidence that COB does interact with other proteins, let alone itself, and further research is needed in this area. In addition, it is unknown if the severe phenotype of Y60A-COB-mcYFP is caused by the inability to bind to cellulose or if the amino acid substitution causes significant alteration to the folding of the protein.

Chapter 6: Conclusions

6.1 Major findings of this work

For my Master's thesis, I aimed to further our understanding of COBRA's role in cellulose biosynthesis. Despite the importance of COB in plant development, little is known about its function, primarily due to the difficulties in generating viable reporter-fusion constructs for live-cell imaging and biochemical and proteomic assays. Therefore, my research objectives were to:

1. To improve the COB-cYFP lines for live-cell imaging.

2. To generate a COB-reporter fusion construct that fully complements *cob-4* and to use this to perform biochemical and proteomic analysis.

3. To search for new potential functional domains in COB.

In Chapter 3, I showed that the radial swelling phenotype in the original COB-dcYFP line was likely caused by the dimerization of the cYFP. Site-directed mutagenesis of the cYFP to prevent dimerization in order to create COB-mcYFP resulted in significantly stronger complementation the *cob-4* null mutant, though minor radial swelling was still present. Furthermore, I created COB-mcYFP lines crossed with the endosomal marker lines wave_12R and wave2R in order to help discern if the puncta seen in live-cell imaging were endocytic, in addition to creating lines lacking root hairs in order to allow easier usage of drugs during live-cell imaging. From examining cell wall protein extracts I was unable to detect COB-mcYFP in cell wall extracts, suggesting that the addition of mcYFP may interfere with its function. In addition, I demonstrated that over-expression of the COB-mcYFP construct is not able to rescue *cob-4* and caused defects in silique production and seed setting.

In chapter 4, I showed the ability of a 6x-histidine tagged COB construct, HisCOB, to fully complement the *cob-4* null mutant. HisCOB had the tag inserted at different location than the COB-cYFP constructs, as insertion of 6x-His at the cYFP site yielded no viable transformants. I demonstrated that HisCOB, unlike COB-mcYFP, was found in the cell wall following extraction of cell wall proteins. However, the analysis of these cell wall extracts also suggested that HisCOB underwent at least two cleavage events within the cell wall.

The first of the cleavage events appears to happen once HisCOB is bound to the cellulose microfibrils and acts to release HisCOB from the plasma membrane. While it is not obvious if this cleavage simply involves removal of the GPI-anchor or removal of part of the protein, members of the COB gene family have previously been shown to be affected by phospholipase D (L. Liu et al., 2013). Once released from the plasma membrane, HisCOB might therefore remain bound to cellulose microfibrils for an indeterminate amount of time before undergoing a second cleavage event.

The second cleavage event appears to occur downstream of the cellulose-binding domain, releasing a COB peptide of around 33 kDa. This peptide is most likely to interact with and/or bind to other cell wall proteins, as it is able to remain in the cell wall protein fraction during extraction. Furthermore, this 33 kDa peptide is likely endocytosed back in to the cell as it is consistently found in cytoplasmic protein extracts. While it is still unknown what the exact function of this peptide is, it does give credence to the model where COB functions as a cell wall sensor and transcriptional regulator by providing a mechanistic link between COB's cell wall localization and interactions with cytoplasmic signal transduction cascades.

In chapter 5, the sucrose-dependent radial swelling phenotype of HisCOB, *hulk-1*, and *cob-1* were explored, and it is suggested that amino acids 104 – 186 play an important role in

COB's function. I also provide evidence that COB may function as a homodimer by examining HisCOB x *cob-1* transheterozygotes, which show an intermediate sucrose-dependent phenotype compared to the single lines. Finally, immunoblotting experiments indicate that HisCOB's conditional phenotype on high sucrose is not likely caused by perturbations in its ability to be cleaved.

In order to further explore if COB functions as a heterodimer, I examined wild types lines that were transformed with gCOB, HisCOB, and COB-mcYFP. Neither gCOB nor HisCOB showed phenotypes when transformed into wild type, suggesting that COB gene dosage does not have obvious effects on root growth. However, when expressed in the wild-type background, COB-mcYFP led to reductions in root length, suggesting that there is some negative interaction between COB-mcYFP and the endogenous, wild-type COB. Similarly, transformation of wild type with Y60A-COB-mcYFP, a COB-mcYFP variant lacking a functional cellulose-binding domain, caused dominant-negative phenotype with radial swelling in both the primary and the lateral roots. This dominant-negative phenotype suggests that Y60A-COB-mcYFP may severely interfere with the function of the endogenous, wild-type COB.

6.2 Outstanding Questions and Future Directions

6.2.1 Determining the function of the 33 kDa peptide

While I predicted that the cleaved, endocytosed 33 kDa peptide is important for the function of COB, much work still needs to be done in this area. The first step is to determine the exact amino acid sequence of the 33 kDa peptide, as the work shown in chapter 4 only provides an estimate of the peptide sequence. Once the exact sequence is determined, it would then be possible to mutate the cleavage site(s) in order to generate uncleavable COB constructs, which can then be transformed into *cob-4* null mutants to examine their viability. In addition, it would

be possible to constitutively express or over-express, using UBQ*pro* or 35S*pro* respectively, the cleaved peptide sequence and examine their effects on growth anisotropy and cellulose biosynthesis.

6.2.2 The transcriptional role of COBRA

While there is growing evidence that COB likely has a transcriptional role rather than a structural role in relation to cellulose biosynthesis, it is not known if and what genes are mis-regulated in various *cob* mutants. To address this, transcriptome analysis of various *cob* mutants under different conditions using RNA sequencing (RNAseq) could yield significant insight into the exact function on COB. For example, the addition of 4.5% sucrose to *cob-1* mutants induces a drastic change in growth anisotropy and cellulose content, but it is not known what genes contribute to this phenotype. For example, while COB and the primary CESAs are known to be highly co-expressed, it is unknown if the cellulose deficiencies seen in COB mutants is due to changes in CESA expression.

In addition, recent findings in the Wasteneys lab have identified two chemicals that are able to alleviate the *cob-1* conditional phenotype on 4.5% sucrose: the aspartyl protease inhibitor pepstatin and the *Streptomyces scabies* toxin Thaxtomin A (TA). While TA severely hinders the growth of all lines on 0% sucrose medium, it can alleviate the conditional radial swelling of *cob-1* on 4.5% sucrose-containing medium. Pepstatin has also been shown to have an effect on COB, suggesting a role of aspartyl proteases in COB function. Pepstatin alleviates the conditional radial swelling of *cob-1* on 4.5% sucrose-containing medium, while it slightly reduces the growth all lines on 0% sucrose medium. RNAseq analysis of these chemical treatments could yield new insight into COB's function in cellulose biosynthesis.

6.2.3 Investigating cellulose crystallinity and degree of pectin methylesterifcation in COB mutants

While the conditional radial swelling of *cob-1* has been well established, and my previous work has shown that HisCOB also exhibits a similar phenotype, the cause of this loss of growth anisotropy in relation to primary cell wall composition is unknown. By using antibodies targeting crystalline and amorphous cellulose, it would be possible to examine the cellulose composition of the primary cell wall using transmission electron microscopy (TEM). Alternatively, cellulose crystallinity could also be determined using techniques such as X-ray diffraction or solid-state ^{13}C nuclear magnetic resonance.

While there is a growing body of work demonstrating the importance of pectins in maintaining cell wall integrity and growth anisotropy (Bethke et al., 2016; Höfte, Peaucelle, & Braybrook, 2012; Torode et al., 2017) in addition to a link between COB and pectin methylesterification (Sorek et al., 2015), little is known about the relationship between pectin and COB. By using antibodies specific to esterified and de-esterified pectins, it would be possible to probe *cob* mutants for changes in the degree of the pectin methylesterification during radial swelling, such as in the case of *cob-1* on 4.5% sucrose containing medium. Alternatively, atomic force microscopy could also be used to detect stiffness changes in pectins during radial swelling.

6.2.4 Identification of COBRA-interacting proteins

As my work has shown that COB is likely to interact with other cell wall proteins, identification of these unknown proteins is of key importance. The low abundance of COB in the plant cell, however, has made sequencing using mass spectrometry a challenge and poses a significant challenge for identification of COB-interactors. A possible technique that could

accomplish this task is *in planta* chemical cross-linking, which has previously been demonstrated to be a viable method to identify even transient protein-protein interactors (Zhu et al., 2016). Alternatively, there is growing popularity in use of recombinant ligases conjugated to the protein of interest to tag other close-proximity proteins. For example, the biotin ligase system has been shown to be viable in identifying protein-protein interactions in mammalian systems, though its viability in plants is still unknown (Kim et al., 2016; Roux, Kim, Raida, & Burke, 2012).

Bibliography

Atmodjo, M. A., Hao, Z., & Mohnen, D. (2013). Evolving views of pectin biosynthesis. *Annu Rev Plant Biol*, *64*, 747–779. https://doi.org/10.1146/annurev-arplant-042811-105534

Ben-Tov, D., Idan-Molakandov, A., Hugger, A., Ben-Shlush, I., Günl, M., Yang, B., … Harpaz-Saad, S. (2018). The role of COBRA-LIKE 2 function, as part of the complex network of interacting pathways regulating Arabidopsis seed mucilage polysaccharide matrix organization. *The Plant Journal*, n/a-n/a. https://doi.org/10.1111/tpj.13871

Benfey, P. N., Linstead, P. J., Roberts, K., Schiefelbein, J. W., Hauser, M. T., & Aeschbacher, R. A. (1993). Root development in Arabidopsis: four mutants with dramatically altered root morphogenesis. *Development*, *119*(1), 57–70.

Bethke, G., Thao, A., Xiong, G., Li, B., Soltis, N. E., Hatsugai, N., … Glazebrook, J. (2016). Pectin Biosynthesis Is Critical for Cell Wall Integrity and Immunity in Arabidopsis thaliana. *Plant Cell*, *28*(2), 537–556. https://doi.org/10.1105/tpc.15.00404

Block, H., Maertens, B., Spriestersbach, A., Brinker, N., Kubicek, J., Fabis, R., … Schäfer, F. (2009). Chapter 27 Immobilized-Metal Affinity Chromatography (IMAC): A Review. In R. R. Burgess & M. P. B. T.-M. in E. Deutscher (Eds.), *Guide to Protein Purification, 2nd Edition* (Vol. 463, pp. 439–473). Academic Press. https://doi.org/https://doi.org/10.1016/S0076-6879(09)63027-5

Borner, G. H. H., Lilley, K. S., Stevens, T. J., & Dupree, P. (2003). Identification of Glycosylphosphatidylinositol-Anchored Proteins in Arabidopsis. A Proteomic and Genomic Analysis. *Plant Physiology*, *132*(2), 568 LP-577. Retrieved from http://www.plantphysiol.org/content/132/2/568.abstract

Brady, S. M., Song, S., Dhugga, K. S., Rafalski, J. A., & Benfey, P. N. (2007). Combining

expression and comparative evolutionary analysis: the COBRA gene family. *Plant Physiol*, *143*. https://doi.org/10.1104/pp.106.087262

Burn, J. E., Hocart, C. H., Birch, R. J., Cork, A. C., & Williamson, R. E. (2002). Functional Analysis of the Cellulose Synthase Genes CesA1, CesA2, and CesA3 in Arabidopsis. *Plant Physiology*, *129*(2), 797–807. https://doi.org/10.1104/pp.010931

Caffall, K. H., & Mohnen, D. (2009). The structure, function, and biosynthesis of plant cell wall pectic polysaccharides. *Carbohydr Res*, *344*(14), 1879–1900. https://doi.org/10.1016/j.carres.2009.05.021

Candiano, G., Bruschi, M., Musante, L., Santucci, L., Ghiggeri, G. M., Carnemolla, B., … Righetti, P. G. (2004). Blue silver: A very sensitive colloidal Coomassie G-250 staining for proteome analysis. *ELECTROPHORESIS*, *25*(9), 1327–1333. https://doi.org/10.1002/elps.200305844

Cao, Y., Tang, X., Giovannoni, J., Xiao, F., & Liu, Y. (2012). Functional characterization of a tomato COBRA-likegene functioning in fruit development and ripening. *BMC Plant Biology*, *12*(1), 211. https://doi.org/10.1186/1471-2229-12-211

Cavalier, D. M., Lerouxel, O., Neumetzler, L., Yamauchi, K., Reinecke, A., Freshour, G., … Keegstra, K. (2008). Disrupting two Arabidopsis thaliana xylosyltransferase genes results in plants deficient in xyloglucan, a major primary cell wall component. *Plant Cell*, *20*(6), 1519–1537. https://doi.org/10.1105/tpc.108.059873

Clough, S., & Bent, A. (2008). Floral dip: a simplified method for Agrobacterium -mediated transformation of Arabidopsis thaliana. *The Plant Journal*, *16*(6), 735–743. https://doi.org/10.1046/j.1365-313x.1998.00343.x

Coleman, H. D., Yan, J., & Mansfield, S. D. (2009). Sucrose synthase affects carbon partitioning

to increase cellulose production and altered cell wall ultrastructure. *Proceedings of the National Academy of Sciences*, *106*(31), 13118–13123. https://doi.org/10.1073/pnas.0900188106

Cosgrove, D. J. (2000). Loosening of plant cell walls by expansins. *Nature*, *407*. https://doi.org/10.1038/35030000

Cosgrove, D. J. (2005). Growth of the plant cell wall. *Nat Rev Mol Cell Biol*, *6*(11), 850–861. https://doi.org/10.1038/nrm1746

Cosgrove, D. J. (2014). Re-constructing our models of cellulose and primary cell wall assembly. *Curr Opin Plant Biol*, *22*, 122–131. https://doi.org/10.1016/j.pbi.2014.11.001

Day, R. N., & Davidson, M. W. (2009). The fluorescent protein palette: tools for cellular imaging. *Chemical Society Reviews*, *38*(10), 2887–2921. https://doi.org/10.1039/b901966a

DeBruine, Z. J., Ke, J., Harikumar, K. G., Gu, X., Borowsky, P., Williams, B. O., … Melcher, K. (2017). Wnt5a promotes Frizzled-4 signalosome assembly by stabilizing cysteine-rich domain dimerization. *Genes & Development*, *31*(9), 916–926. https://doi.org/10.1101/gad.298331.117

Desprez, T., Juraniec, M., Crowell, E. F., Jouy, H., Pochylova, Z., Parcy, F., … Vernhettes, S. (2007). Organization of cellulose synthase complexes involved in primary cell wall synthesis in Arabidopsis thaliana *Proceedings of the National Academy of Sciences*, *104*(39), 15572 LP-15577. Retrieved from http://www.pnas.org/content/104/39/15572.abstract

Diotallevi, F., & Mulder, B. (2007). The cellulose synthase complex: a polymerization driven supramolecular motor. *Biophys J*, *92*(8), 2666–2673. https://doi.org/10.1529/biophysj.106.099473

Edwards, K., Johnstone, C., & Thompson, C. (1991). A simple and rapid method for the preparation of plant genomic DNA for PCR analysis. *Nucleic Acids Research*, *19*(6), 1349. Retrieved from http://www.ncbi.nlm.nih.gov/pmc/articles/PMC333874/

Feiz, L., Irshad, M., F Pont-Lezica, R., Canut, H., & Jamet, E. (2006). Evaluation of cell wall preparations for proteomics: a new procedure for purifying cell walls from Arabidopsis hypocotyls. *Plant Methods*, *2*(1), 10. https://doi.org/10.1186/1746-4811-2-10

Fernandes, A. N., Thomas, L. H., Altaner, C. M., Callow, P., Forsyth, V. T., Apperley, D. C., … Jarvis, M. C. (2011). Nanostructure of cellulose microfibrils in spruce wood. *Proceedings of the National Academy of Sciences*, *108*(47), E1195 LP-E1203. Retrieved from http://www.pnas.org/content/108/47/E1195.abstract

Fujita, M., Himmelspach, R., Hocart, C. H., Williamson, R. E., Mansfield, S. D., & Wasteneys, G. O. (2011). Cortical microtubules optimize cell-wall crystallinity to drive unidirectional growth in Arabidopsis. *Plant J*, *66*(6), 915–928. https://doi.org/10.1111/j.1365-313X.2011.04552.x

Fujita, M., Himmelspach, R., Ward, J., Whittington, A., Hasenbein, N., Liu, C., … Wasteneys, G. O. (2013). The anisotropy1 D604N mutation in the Arabidopsis cellulose synthase1 catalytic domain reduces cell wall crystallinity and the velocity of cellulose synthase complexes. *Plant Physiol*, *162*(1), 74–85. https://doi.org/10.1104/pp.112.211565

Fujita, M., Lechner, B., Barton, D. A., Overall, R. L., & Wasteneys, G. O. (2012). The missing link: Do cortical microtubules define plasma membrane nanodomains that modulate cellulose biosynthesis? *Protoplasma*, *249*(SUPPL. 1), 59–67. https://doi.org/10.1007/s00709-011-0332-z

Geldner, N., Dénervaud-Tendon, V., Hyman, D. L., Mayer, U., Stierhof, Y.-D., & Chory, J.

(2009). Rapid, combinatorial analysis of membrane compartments in intact plants with a multicolor marker set. *The Plant Journal : For Cell and Molecular Biology*, *59*(1), 169–178. https://doi.org/10.1111/j.1365-313X.2009.03851.x

Gibson, D. G., Young, L., Chuang, R.-Y., Venter, J. C., Hutchison III, C. A., & Smith, H. O. (2009). Enzymatic assembly of DNA molecules up to several hundred kilobases. *Nature Methods*, *6*, 343. Retrieved from http://dx.doi.org/10.1038/nmeth.1318

Gu, Y., Kaplinsky, N., Bringmann, M., Cobb, A., Carroll, A., Sampathkumar, A., … Somerville, C. R. (2010). Identification of a cellulose synthase-associated protein required for cellulose biosynthesis. *Proceedings of the National Academy of Sciences*, *107*(29), 12866–12871. https://doi.org/10.1073/pnas.1007092107

Guerriero, G., Fugelstad, J., & Bulone, V. (2010). What Do We Really Know about Cellulose Biosynthesis in Higher Plants ?, *52*(2), 161–175. https://doi.org/10.1111/j.1744-7909.2010.00935.x

Hallac, B. B., & Ragauskas, A. J. (2011). Analyzing cellulose degree of polymerization and its relevancy to cellulosic ethanol. *Biofuels, Bioproducts and Biorefining*, *5*(2), 215–225. https://doi.org/10.1002/bbb.269

Hanahan, D. (1983). Studies on transformation of Escherichia coli with plasmids. *Journal of Molecular Biology*, *166*(4), 557–580. https://doi.org/https://doi.org/10.1016/S0022-2836(83)80284-8

Harris, D. M., Corbin, K., Wang, T., Gutierrez, R., Bertolo, A. L., Petti, C., … DeBolt, S. (2012). Cellulose microfibril crystallinity is reduced by mutating C-terminal transmembrane region residues CESA1A903V and CESA3T942I of cellulose synthase. *Proceedings of the National Academy of Sciences*, *109*(11), 4098–4103.

https://doi.org/10.1073/pnas.1200352109

Hauser, M. T., Morikami, A., & Benfey, P. N. (1995). Conditional root expansion mutants of Arabidopsis. *Development (Cambridge, England)*, *121*(4), 1237–1252.

Hayashi, T. (1989). Xyloglucans in the Primary Cell Wall. *Annual Review of Plant Physiology and Plant Molecular Biology*, *40*(1), 139–168. https://doi.org/doi:10.1146/annurev.pp.40.060189.001035

Höfte, H., Peaucelle, A., & Braybrook, S. (2012). Cell wall mechanics and growth control in plants: the role of pectins revisited . *Frontiers in Plant Science* . Retrieved from https://www.frontiersin.org/article/10.3389/fpls.2012.00121

Kim, D. I., Jensen, S. C., Noble, K. A., Kc, B., Roux, K. H., Motamedchaboki, K., & Roux, K. J. (2016). An improved smaller biotin ligase for BioID proximity labeling. *Molecular Biology of the Cell*. https://doi.org/10.1091/mbc.E15-12-0844

Ko, J. H., Kim, J. H., Jayanty, S. S., Howe, G. A., & Han, K. H. (2006). Loss of function of COBRA, a determinant of oriented cell expansion, invokes cellular defence responses in Arabidopsis thaliana. *Journal of Experimental Botany*, *57*(12), 2923–2936. https://doi.org/10.1093/jxb/erl052

Lane, D. R., Wiedemeier, A., Peng, L., Höfte, H., Vernhettes, S., Desprez, T., … Williamson, R. E. (2001). Temperature-Sensitive Alleles of RSW2 Link the KORRIGAN Endo-1,4-β-Glucanase to Cellulose Synthesis and Cytokinesis in Arabidopsis. *Plant Physiology*, *126*(1), 278–288. Retrieved from http://www.ncbi.nlm.nih.gov/pmc/articles/PMC102302/

Laurie, G. S., & David, G. O. (2005). SPATIAL CONTROL OF CELL EXPANSION BY THE PLANT CYTOSKELETON. *Annual Review of Cell and Developmental Biology*, *21*(1), 271–295. https://doi.org/doi:10.1146/annurev.cellbio.21.122303.114901

Li, S., Bashline, L., Lei, L., & Gu, Y. (2014). Cellulose Synthesis and Its Regulation. *The Arabidopsis Book / American Society of Plant Biologists*, *12*, e0169. https://doi.org/10.1199/tab.0169

Li, S., Ge, F.-R., Xu, M., Zhao, X.-Y., Huang, G.-Q., Zhou, L.-Z., … Zhang, Y. (2013). Arabidopsis COBRA-LIKE 10, a GPI-anchored protein, mediates directional growth of pollen tubes. *The Plant Journal*, *74*(3), 486–497. https://doi.org/10.1111/tpj.12139

Li, Y., Qian, Q., Zhou, Y., Yan, M., Sun, L., Zhang, M., … Li, J. (2003). BRITTLE CULM1, which encodes a COBRA-like protein, affects the mechanical properties of rice plants. *Plant Cell*, *15*. https://doi.org/10.1105/tpc.011775

Lionetti, V., Cervone, F., & Bellincampi, D. (2012). Methyl esterification of pectin plays a role during plant-pathogen interactions and affects plant resistance to diseases. *J Plant Physiol*, *169*(16), 1623–1630. https://doi.org/10.1016/j.jplph.2012.05.006

Liu, L., Shang-Guan, K., Zhang, B., Liu, X., Yan, M., Zhang, L., … Zhou, Y. (2013). Brittle Culm1, a COBRA-Like Protein, Functions in Cellulose Assembly through Binding Cellulose Microfibrils. *PLoS Genetics*, *9*(8). https://doi.org/10.1371/journal.pgen.1003704

Liu, Z., Schneider, R., Kesten, C., Zhang, Y., Somssich, M., Zhang, Y., … Persson, S. (2016). Cellulose-Microtubule Uncoupling Proteins Prevent Lateral Displacement of Microtubules during Cellulose Synthesis in Arabidopsis. *Dev Cell*, *38*(3), 305–315. https://doi.org/http://dx.doi.org/10.1016/j.devcel.2016.06.032

Mauldin, J. P., Lu, M., Das, S., Park, D., Ernst, P. B., & Ravichandran, K. S. (2013). A link between the cytoplasmic engulfment protein Elmo1 and the Mediator complex subunit Med31. *Current Biology : CB*, *23*(2), 162–167. https://doi.org/10.1016/j.cub.2012.11.049

McNamara, J. T., Morgan, J. L., & Zimmer, J. (2015). A molecular description of cellulose

biosynthesis. *Annu Rev Biochem*, *84*, 895–921. https://doi.org/10.1146/annurev-biochem-060614-033930

Meijering, E., Jacob, M., Sarria, J. -C. ., Steiner, P., Hirling, H., & Unser, M. (2004). Design and validation of a tool for neurite tracing and analysis in fluorescence microscopy images. *Cytometry Part A*, *58A*(2), 167–176. https://doi.org/10.1002/cyto.a.20022

Mohnen, D. (2008). Pectin structure and biosynthesis. *Curr Opin Plant Biol*, *11*(3), 266–277. https://doi.org/10.1016/j.pbi.2008.03.006

Montague, T. G., Cruz, J. M., Gagnon, J. A., Church, G. M., & Valen, E. (2014). CHOPCHOP: a CRISPR/Cas9 and TALEN web tool for genome editing. *Nucleic Acids Research*, *42*(Web Server issue), W401–W407. https://doi.org/10.1093/nar/gku410

Newman, R. H., Hill, S. J., & Harris, P. J. (2013). Wide-Angle X-Ray Scattering and Solid-State Nuclear Magnetic Resonance Data Combined to Test Models for Cellulose Microfibrils in Mung Bean Cell Walls. *Plant Physiology*, *163*(4), 1558 LP-1567. Retrieved from http://www.plantphysiol.org/content/163/4/1558.abstract

Nühse, T. S., Stensballe, A., Jensen, O. N., & Peck, S. C. (2004). Phosphoproteomics of the Arabidopsis Plasma Membrane and a New Phosphorylation Site Database. *The Plant Cell*, *16*(9), 2394 LP-2405. Retrieved from http://www.plantcell.org/content/16/9/2394.abstract

Park, Y. B., & Cosgrove, D. J. (2012). A revised architecture of primary cell walls based on biomechanical changes induced by substrate-specific endoglucanases. *Plant Physiol*, *158*(4), 1933–1943. https://doi.org/10.1104/pp.111.192880

Persson, S., Wei, H., Milne, J., Page, G. P., & Somerville, C. R. (2005). Identification of genes required for cellulose synthesis by regression analysis of public microarray data sets. *Proceedings of the National Academy of Sciences of the United States of America*, *102*(24),

8633 LP-8638. Retrieved from http://www.pnas.org/content/102/24/8633.abstract

Popper, Z. A., Michel, G., Herve, C., Domozych, D. S., Willats, W. G., Tuohy, M. G., … Stengel, D. B. (2011). Evolution and diversity of plant cell walls: from algae to flowering plants. *Annu Rev Plant Biol*, *62*, 567–590. https://doi.org/10.1146/annurev-arplant-042110-103809

Printz, B., Dos Santos Morais, R., Wienkoop, S., Sergeant, K., Lutts, S., Hausman, J.-F., & Renaut, J. (2015). An improved protocol to study the plant cell wall proteome. *Frontiers in Plant Science*, *6*, 237. https://doi.org/10.3389/fpls.2015.00237

Ridley, B. L., O'Neill, M. A., & Mohnen, D. (2001). Pectins: structure, biosynthesis, and oligogalacturonide-related signaling. *Phytochemistry*, *57*(6), 929–967. https://doi.org/http://dx.doi.org/10.1016/S0031-9422(01)00113-3

Ringli, C., Baumberger, N., & Keller, B. (2005). The Arabidopsis Root Hair Mutants der2–der9 are Affected at Different Stages of Root Hair Development. *Plant and Cell Physiology*, *46*(7), 1046–1053. Retrieved from http://dx.doi.org/10.1093/pcp/pci115

Roudier, F., Fernandez, A. G., Fujita, M., Himmelspach, R., Borner, G. H., Schindelman, G., … Benfey, P. N. (2005). COBRA, an Arabidopsis extracellular glycosyl-phosphatidyl inositol anchored protein, specifically controls highly anisotropic expansion through its involvement in cellulose microfibril orientation. *Plant Cell*, *17*. https://doi.org/10.1105/tpc.105.031732

Roudier, F., Schindelman, G., DeSalle, R., & Benfey, P. N. (2002). The COBRA family of putative GPI-anchored proteins in Arabidopsis: a new fellowship in expansion. *Plant Physiol*, *130*. https://doi.org/10.1104/pp.007468

Roux, K. J., Kim, D. I., Raida, M., & Burke, B. (2012). A promiscuous biotin ligase fusion protein identifies proximal and interacting proteins in mammalian cells. *Journal of Cell*

Biology, *196*(6), 801–810. https://doi.org/10.1083/jcb.201112098

Scheller, H. V, & Ulvskov, P. (2010). Hemicelluloses. *Annu Rev Plant Biol*, *61*, 263–289. https://doi.org/10.1146/annurev-arplant-042809-112315

Schindelin, J., Arganda-Carreras, I., Frise, E., Kaynig, V., Longair, M., Pietzsch, T., … Cardona, A. (2012). Fiji: an open-source platform for biological-image analysis. *Nature Methods*, *9*, 676. Retrieved from http://dx.doi.org/10.1038/nmeth.2019

Schindelman, G., Morikami, A., Jung, J., Baskin, T. I., Carpita, N. C., Derbyshire, P., … Benfey, P. N. (2001). COBRA encodes a putative GPI-anchored protein, which is polarly localized and necessary for oriented cell expansion in Arabidopsis. *Genes Dev*, *15*. https://doi.org/10.1101/gad.879101

Schlessinger, J. (2002). Ligand-Induced, Receptor-Mediated Dimerization and Activation of EGF Receptor. *Cell*, *110*(6), 669–672. https://doi.org/https://doi.org/10.1016/S0092-8674(02)00966-2

Shevchenko, A., Wilm, M., Vorm, O., & Mann, M. (1996). Mass Spectrometric Sequencing of Proteins from Silver-Stained Polyacrylamide Gels, *68*(5), 850–858. https://doi.org/10.1021/ac950914h

Simossis, V. A., & Heringa, J. (2005). PRALINE: a multiple sequence alignment toolbox that integrates homology-extended and secondary structure information. *Nucleic Acids Research*, *33*(Web Server issue), W289–W294. https://doi.org/10.1093/nar/gki390

Smulski, C. R., Beyrath, J., Decossas, M., Chekkat, N., Wolff, P., Estieu-Gionnet, K., … Fournel, S. (2013). Cysteine-rich Domain 1 of CD40 Mediates Receptor Self-assembly. *The Journal of Biological Chemistry*, *288*(15), 10914–10922. https://doi.org/10.1074/jbc.M112.427583

Sorek, N., Ryan, A., Carroll, A., & Somerville, C. (2016). Functional analysis of the COBRA-like family. *PeerJ PrePrints*, *4*, e1740v1. https://doi.org/10.7287/peerj.preprints.1740v1

Sorek, N., Szemenyei, H., Sorek, H., Landers, A., Knight, H., Bauer, S., … Somerville, C. R. (2015). Identification of MEDIATOR16 as the *Arabidopsis* COBRA suppressor MONGOOSE1. *Proceedings of the National Academy of Sciences*, *112*(52), 201521675. https://doi.org/10.1073/pnas.1521675112

Timmers, J., Vernhettes, S., Desprez, T., Vincken, J.-P., Visser, R. G. F., & Trindade, L. M. (2009). Interactions between membrane-bound cellulose synthases involved in the synthesis of the secondary cell wall. *FEBS Letters*, *583*(6), 978–982. https://doi.org/https://doi.org/10.1016/j.febslet.2009.02.035

Torode, T. A., O'Neill, R. E., Marcus, S. E., Cornuault, V., Pose-Albacete, S., Lauder, R. P., … Knox, J. P. (2017). Branched pectic galactan in phloem-sieve-element cell walls: implications for cell mechanics. *Plant Physiology*. Retrieved from http://www.plantphysiol.org/content/early/2017/11/17/pp.17.01568.abstract

Vain, T., Crowell, E. F., Timpano, H., Biot, E., Desprez, T., Mansoori, N., … Vernhettes, S. (2014). The Cellulase KORRIGAN Is Part of the Cellulose Synthase Complex. *Plant Physiol*, *165*(4), 1521–1532. https://doi.org/10.1104/pp.114.241216

Wada, T., Kurata, T., Tominaga, R., Koshino-Kimura, Y., Tachibana, T., Goto, K., … Okada, K. (2002). Role of a positive regulator of root hair development, CAPRICE, in Arabidopsis root epidermal cell differentiation. *Development*, *129*(23), 5409–5419. https://doi.org/10.1242/dev.00111

Wang, Z. P., Xing, H. L., Dong, L., Zhang, H. Y., Han, C. Y., Wang, X. C., & Chen, Q. J. (2015). Egg cell-specific promoter-controlled CRISPR/Cas9 efficiently generates

homozygous mutants for multiple target genes in Arabidopsis in a single generation. *Genome Biol*, *16*, 144. https://doi.org/10.1186/s13059-015-0715-0

Wolf, S., Mouille, G., & Pelloux, J. (2009). Homogalacturonan methyl-esterification and plant development. *Mol Plant*, *2*(5), 851–860. https://doi.org/10.1093/mp/ssp066

Xing, H.-L., Dong, L., Wang, Z.-P., Zhang, H.-Y., Han, C.-Y., Liu, B., … Chen, Q.-J. (2014). A CRISPR/Cas9 toolkit for multiplex genome editing in plants. *BMC Plant Biology*, *14*(1), 327. https://doi.org/10.1186/s12870-014-0327-y

Xu, K., Liu, J., Fan, M., Xin, W., Hu, Y., & Xu, C. (2012). A genome-wide transcriptome profiling reveals the early molecular events during callus initiation in Arabidopsis multiple organs. *Genomics*, *100*(2), 116–124. https://doi.org/https://doi.org/10.1016/j.ygeno.2012.05.013

Ye, X., Kang, B., Osburn, L. D., & Cheng, Z.-M. (2009). The COBRA gene family in Populus and gene expression in vegetative organs and in response to hormones and environmental stresses. *Plant Growth Regulation*, *58*(2), 211–223. https://doi.org/10.1007/s10725-009-9369-9

Yin, J., & Wang, G. (2014). The Mediator complex: a master coordinator of transcription and cell lineage development. *Development*, *141*(5), 977 LP-987. Retrieved from http://dev.biologists.org/content/141/5/977.abstract

Zhang, Y., Nikolovski, N., Sorieul, M., Vellosillo, T., McFarlane, H. E., Dupree, R., … Dupree, P. (2016). Golgi-localized STELLO proteins regulate the assembly and trafficking of cellulose synthase complexes in Arabidopsis. *Nature Communications*, *7*, 11656. https://doi.org/10.1038/ncomms11656http://www.nature.com/articles/ncomms11656#supplementary-information

Zhu, X., Yu, F., Yang, Z., Liu, S., Dai, C., Lu, X., … Li, N. (2016). In planta chemical cross-linking and mass spectrometry, 1915–1927. https://doi.org/10.1002/pmic.201500310